A STUDY OF THE EFFECT OF GAMMA IRRADIATION ON CELLULAR METABOLISM BY NUCLEAR MAGNETIC RESONANCE SPECTROSCOPY

A thesis

Presented to

The Faculty of Graduate Studies

of

Lakehead University

By

CURTIS M. SHEWCHUK

In partial fulfillment of requirements

For the degree of

Master of Science

May 3, 2005

© Curtis Shewchuk, 2005

Reproduced with permission of the copyright owner. Further reproduction prohibited without permission.

Library and Archives Canada

Published Heritage Branch

395 Wellington Street
Ottawa ON K1A 0N4
Canada

Bibliothèque et Archives Canada

Direction du Patrimoine de l'édition

395, rue Wellington
Ottawa ON K1A 0N4
Canada

Your file Votre référence
ISBN: 0-494-10670-0
Our file Notre référence
ISBN: 0-494-10670-0

NOTICE:
The author has granted a non-exclusive license allowing Library and Archives Canada to reproduce, publish, archive, preserve, conserve, communicate to the public by telecommunication or on the Internet, loan, distribute and sell theses worldwide, for commercial or non-commercial purposes, in microform, paper, electronic and/or any other formats.

The author retains copyright ownership and moral rights in this thesis. Neither the thesis nor substantial extracts from it may be printed or otherwise reproduced without the author's permission.

AVIS:
L'auteur a accordé une licence non exclusive permettant à la Bibliothèque et Archives Canada de reproduire, publier, archiver, sauvegarder, conserver, transmettre au public par télécommunication ou par l'Internet, prêter, distribuer et vendre des thèses partout dans le monde, à des fins commerciales ou autres, sur support microforme, papier, électronique et/ou autres formats.

L'auteur conserve la propriété du droit d'auteur et des droits moraux qui protège cette thèse. Ni la thèse ni des extraits substantiels de celle-ci ne doivent être imprimés ou autrement reproduits sans son autorisation.

In compliance with the Canadian Privacy Act some supporting forms may have been removed from this thesis.

While these forms may be included in the document page count, their removal does not represent any loss of content from the thesis.

Conformément à la loi canadienne sur la protection de la vie privée, quelques formulaires secondaires ont été enlevés de cette thèse.

Bien que ces formulaires aient inclus dans la pagination, il n'y aura aucun contenu manquant.

Canada

Reproduced with permission of the copyright owner. Further reproduction prohibited without permission.

ABSTRACT

The phenomenon of NMR plays an important role in a number of different scientific and medical fields. Nuclear magnetic resonance has the ability to detect changes in tumour, and cell metabolism caused by both chemotherapy and radiation therapy treatments. This project determined the feasibility of NMR spectroscopy for quantifying the effect of radiation therapy on the cellular metabolite levels of the MCF-7 cancer cell line. The metabolites were extracted using a freeze-thaw procedure developed for this study, and analyzed by ^{31}P NMR spectroscopy. Phosphorous spectra were normalized to the inorganic phosphate peak height, and relative peak height ratios were calculated for all phosphorous metabolites present. The standard deviations found for peak height ratios were determined by performing a control reproducibility study. It was found that the reproducibility of intra-batch samples was much higher than that of inter-batch samples. The percent error values for intra-batch samples ranged from 2.53 % to 7.98 % throughout the different relative metabolite ratios, and for inter-batch samples, the values ranged from 38.61 % to 49.90 %. The post-irradiation times of 2, 24 and 48 hrs were chosen, and the time of 48 hrs was determined to yield the greatest quantitative change. Considering this, a range of doses (4 to 12Gy) was examined at 48 hrs post-irradiation. Through the qualitative examination of the peak ratios for all of the phosphorous metabolites found in MCF-7 extracts, it was found that a direct correlation exists between the amount of irradiation delivered, and the changes in metabolite intensities for the MCF-7 cell line. Therefore, based on these preliminary results, it has been shown that ^{31}P NMR can be used to monitor the effects of radiation therapy, and potentially, can be used to quantify a dose-response relationship.

Reproduced with permission of the copyright owner. Further reproduction prohibited without permission.

ACKNOWLEDGEMENTS

I would like to thank the many people who helped make this thesis possible. First, thank you to the Northern Cancer Research Foundation for providing the funding necessary for this project. Thank you to Dr. Patrick Rapley and Dr. Christine Gottardo for allowing me to participate in this project and supervising me throughout my Masters degree. Thank you for your guidance and support over the course of the last two years; it is much appreciated. Pat, thank you for picking me up and giving me direction when I had no idea where I was going. Dr. G., thank you for being so flexible and open-minded throughout the course of this project. Thank you also to Dr. Peter McGhee and the Thunder Bay Regional Health Sciences Centre for allowing me to do my Masters in conjunction with the Lakehead University. It has been an invaluable experience. Thank you to Dr. John Th'ng and Christina Richard for growing the cell samples and for working with Dr. Rapley and me to alter the samples as necessary. The project really could not have happened without your help. Thank you to Keith Pringnitz for allowing me to spend so much time with his baby (the NMR Spectrometer) and for helping me learn more about the specifics of the machine. Thank you to Dr. Kinrade for offering advice about certain aspects of the project. Your expertise with NMR is appreciated. Thank you also to the faculty and staff of the Lakehead University Chemistry Department for all of their assistance. I have thoroughly enjoyed my studies at Lakehead and am thankful for everything I have learned. Finally, thank you to my wife and family for supporting me, both emotionally and financially, for the last two years. You really are my personal cheerleading squad.

Reproduced with permission of the copyright owner. Further reproduction prohibited without permission.

TABLE OF CONTENTS

	PAGE
ABSTRACT	
ACKNOWLEDGEMENTS	i
TABLE OF CONTENTS	ii
LIST OF TABLES	iv
LIST OF FIGURES	v
LIST OF ABBREVIATIONS	vii
1.0 INTRODUCTION	1
1.1 Cancer Overview	1
1.2 Cancer Treatment	1
1.2.1 Chemotherapy Overview	1
1.2.2 Radiation Therapy Overview	2
1.3 NMR Spectroscopy Overview	3
1.3.1 Cancer Research via NMR Spectroscopy	5
1.3.2 Cellular Metabolites	6
1.4 Chemotherapy Summary	8
1.5 Radiation Therapy Summary	13
1.6 Cellular Metabolite Extraction Summary	19
1.7 Thesis Objective	21
2.0 EXPERIMENTAL	22
2.1 Nuclear Magnetic Resonance Spectroscopy	22
2.2 Cell Culture	23

Reproduced with permission of the copyright owner. Further reproduction prohibited without permission.

2.3 Irradiation Procedure 23

2.4 Freeze-Thaw Extraction 24

3.0 RESULTS AND DISCUSSION 26

3.1 Extraction Procedure 26

3.2 Peak Identification 35

3.3 Metabolite Stabilization 38

3.4 Reproducibility Studies 40

3.5 Preliminary Irradiation Studies 46

4.0 CONCLUSION 58

5.0 FUTURE WORK 59

6.0 REFERENCES 62

Reproduced with permission of the copyright owner. Further reproduction prohibited without permission.

TABLES

TABLE		PAGE
1	Acquisition parameters used for ^{1}H and ^{31}P spectra	22
2	Standard deviations for ATP DDW control samples	29
3	Standard deviations for ATP DDW/Mg^{+2} control samples	29
4	Standard deviations for ATP D_2O/Mg^{+2} [0.63 M] control samples	31
5	Optimization of sonication parameters	33
6	Chart of chemical shifts (experimental and literature)	37
7	Stability of ^{31}P spectra using BSS solvent	39
8	Stability of ^{31}P spectra using D_2O/Mg^{+2} solvent	39
9	Standard deviation for intra-batch experiments	41
10	Percent standard deviation for intra-batch experiments	43
11	Statistics for inter-batch experiments	44
12	Irradiation sample (2 hours post-irradiation) and a control sample	47
13	Quantitative results of 6 Gy samples at 24 & 48 hours	50
14	Quantitative results of 12 Gy samples at 24 & 48 hours	50
15	Quantitative results for the dose range (4, 6, 8, & 12 Gy)	53
16	Quantitative results for the dose range (4.5, 5, 5.5, 6, & 8.5 Gy)	54

Reproduced with permission of the copyright owner. Further reproduction prohibited without permission.

FIGURES

FIGURE		PAGE
1	^{31}P spectra of OVCAR and MCF-7 cell lines	26
2	^{31}P spectra of fixative agents	28
3	^{31}P spectra of MCF-7 cells using different solvents	28
4	^{31}P spectra of MCF-7 cells suspended in DDW Mg^{+2}/25% D_2O	30
5	^{31}P spectra that show the different sonication procedures	31
6	^{1}H spectra that show the different sonication procedures	32
7	^{31}P and ^{1}H spectra of the optimized sonication procedure	33
8	^{31}P and ^{1}H spectra of the sonication procedure after freeze-drying	34
9	^{31}P and ^{1}H spectra of the optimized extraction procedure	35
10	^{31}P spectrum of MCF-7 cells freeze-thaw extract (LEP)	36
11	^{31}P spectrum of MCF-7 cells freeze-thaw extract (HEP)	37
12	^{31}P spectra of an MCF-7 control freeze-thaw extract (time stability)	38
13	^{31}P spectra of the LEP range of control samples (October 14, 2004)	42
14	^{31}P spectra of the HEP range of intra-batch control samples	42
15	^{31}P spectra of the LEP range of inter-batch control samples	45
16	^{31}P spectra of the HEP range of inter-batch control samples	45
17	^{31}P spectra of MCF-7 cell extracts (2 hours post-irradiation)	47
18	^{31}P spectra of MCF-7 cell extracts (24 hours post-irradiation)	48
19	^{31}P spectra of MCF-7 cell extracts (48 hours post-irradiation)	49
20	^{31}P spectra of the LEP range (4, 6, 8, & 12 Gy)	51
21	^{31}P spectra of the HEP range (4, 6, 8, & 12 Gy)	51

Reproduced with permission of the copyright owner. Further reproduction prohibited without permission.

FIGURES

FIGURE		PAGE
22	^{31}P spectra of the LEP range (4.5, 5, 5.5, 6, & 8.5 Gy)	52
23	^{31}P spectra of the HEP range (4.5, 5, 5.5, 6, & 8.5 Gy)	52
24	A linear fit of the P_i/PE ratio for both irradiation experiments	55
25	A linear fit of the P_i/PC ratio for both irradiation experiments	55
26	A linear fit of the P_i/GPE ratio for both irradiation experiments	56
27	A linear fit of the P_i/GPC ratio for both irradiation experiments	56
28	A linear fit of the P_i/HEP1 ratio for both irradiation experiments	57
29	A linear fit of the P_i/HEP2 ratio for both irradiation experiments	57

Reproduced with permission of the copyright owner. Further reproduction prohibited without permission.

ABBREVIATIONS

ADP	Adenosine Diphosphate
ADR	Adriamycin-Resistant Cell Line
AMP	Adenosine Monophosphate
3-APP	3-aminopropylphosphonate
ATP	Adenosine Triphosphate
BSS	Balanced Salt Solution
Ch	Choline
CNS	Central Nervous System
Cr	Creatine
DDW	Distilled De-ionized Water
D_2O	Deuterium Oxide
2-DG	2-Deoxy-D-Glucose
DMEM	Dulbecco's Modified Eagle's Medium
DNA	Deoxyribonucleic Acid
DPDE	Diphosphodiester
DPE	Dual-Phase Extraction
EDTA	Ethylenediaminetetraacetic Acid
F6P	Fructose-6-Phosphate
G6P	Glucose-6-Phosphate
GPC	Glycerophosphocholine
GPE	Glycerophosphoethanolamine
HEP	High Energy Phosphates
Lac	Lactate
LEP	Low Energy Phosphates
MB231	Human Breast Cancer Cell Line Variant
MCa	Mammary Carcinoma
MCF-7	Human Breast Cancer Cell Line
MDR	Multidrug-Resistance
Meth-A	Methylcholanthrene-Induced Fibrosarcoma
NAA	N-acetylaspartate
NMR	Nuclear Magnetic Resonance
NDP	Nucleotide Diphosphate
NMP	Nucleotide Monophosphate
NTP	Nucleotide Triphosphate
3-O-MG	3-O-methyl-D-glucose
OVCAR	Human Ovarian Cancer Cell Line
PBS	Phosphate Buffer Saline Solution

Reproduced with permission of the copyright owner. Further reproduction prohibited without permission.

PCr	Phosphocreatine
PCA	Perchloric Acid Extract
PC	Phosphocholine
PDE	Phosphodiester
PDR	Pleiotropic Drug Resistance
PE	Phosphoethanolamine
pH_i	Intracellular pH
pH_e	Extracellular pH
P_i	Inorganic Phosphate
PME	Phosphomonoester
PPM	Parts Per Million
RIF-1	Radiation-Induced Fibrosarcoma-1
SCC	Squamous Cell Carcinoma
SD	Standard Deviation
S/N	Signal-to-Noise
SSD	Source to Surface Distance
T1	Spin-Lattice Relaxation Time
UDPS	Uridine Diphosphosugar
UTP	Uridine Triphosphate
WT	Wild Type Human Breast Cancer Cell Line

Reproduced with permission of the copyright owner. Further reproduction prohibited without permission.

1.0 INTRODUCTION:

1.1 Cancer Overview

The Greek physician Hippocrates described cancer as a crablike disease that spreads throughout the body, eventually cutting off life [1]. Today, the term cancer refers to a group of more than 100 different diseases characterized by uncontrolled growth and spread of abnormal cells [2]. Cancer, a disease that has no limitations, attacks every race, age, and sex, and is global. It is estimated that about 134,000 Canadians develop some type of cancer annually [3], and approximately 1,368,030 Americans will be diagnosed in 2004 [2]. For newly diagnosed cases, only about half of the treatments will be successful, resulting in a very high morality rate. The United Kingdom currently attributes 1 in every 5 deaths to cancer [4]. Approximately 69,500 Canadians are expected to die of cancer in 2005, which equates to more than 1,300 people a week [3]. Of the available treatment methods, two of the most commonly used are chemotherapy and radiation therapy.

1.2 Cancer Treatment

1.2.1 Chemotherapy Overview

The term chemotherapy literally means a method of treating a disease using drugs or medications. Cancer chemotherapy is the use of cytotoxic drugs, also known as anticancer or cell-poisoning drugs, to treat cancer. The use of chemotherapy drugs dates at least as far back in history as the 17^{th} and 18^{th} centuries, when belladonna, antimony and arsenic were employed to treat cancer [4]. Currently, there are more than 50 different drugs used for chemotherapy. Cytotoxic drugs act by interfering with the process of cell division and therefore, are most effective on rapidly dividing cells. Cancer cells divide

Reproduced with permission of the copyright owner. Further reproduction prohibited without permission.

much more rapidly than normal cells, which makes chemotherapy a successful way of treating cancer. Unfortunately, normal cells can also be damaged. Therefore, a careful balance between toxicity to the tumor and toxicity to the patient's normal tissues has to be maintained.

1.2.2 Radiation Therapy Overview

Radiation therapy, also known as radiotherapy and x-ray therapy, is defined as the use of ionizing radiation to kill cancer cells and shrink tumors [5]. The first patient cured by radiation therapy was reported in 1899, and in 1922, at the International Congress of Oncology in Paris [6], the medical discipline of clinical radiation therapy began. In the last two decades, there has been a large growth in the knowledge of radiation physics, radiation biology, and clinical treatment planning, allowing for considerable advancements in the treatment of cancer.

Radiobiology is the scientific study of the effects of ionizing radiation on cells and tissues [4]. Radiation is particularly lethal to cells during mitosis [4], and can result in cell death or loss of reproductive capacity. The exact identity of the vital structures, or critical targets, that must be damaged in this mechanism is still unknown [7]. However, it is generally accepted that the specific target of radiation damage is the deoxyribonucleic acid (DNA) molecule that is contained within the chromosomes of the cell's nucleus. When radiation is absorbed in biological material, there is a possibility that it will interact directly with the critical targets in the cell. Radiation has both direct and indirect effects at the molecular level [7]. A direct action of radiation occurs when the atoms of the target become ionized or excited, which initiates a chain of events that leads to a biological change. An indirect action of radiation results when the radiation may interact with other

Reproduced with permission of the copyright owner. Further reproduction prohibited without permission.

atoms or molecules in the cell to produce free radicals that are able to diffuse far enough to reach and damage critical targets. Indirect action damage is more predominant in radiation therapy. For example, a water molecule may become ionized upon interaction with a photon (x-rays or γ-rays) or a charged particle (electron or proton). The ion that is formed has an extremely short lifetime (~ 10^{-10} s), and the result of its decay is a free radical with no charge. The radical can react with another water molecule to form a highly reactive hydroxyl radical $OH^{\cdot}$ that can diffuse a short distance to reach a critical target in a cell. This hydroxyl radical is estimated to cause two thirds of the x-ray damage to DNA in mammalian cells [7].

For any given area that is being treated with radiation therapy, both cancer cells and normal cells will be injured or destroyed. Therefore, as in the case of chemotherapy, radiation therapy relies on the fact that most normal cells can recover from the effects of radiation and regain function more quickly than cancer cells. A careful balance has to be maintained between the toxicity delivered to the tumor and that delivered to the patient's normal tissues. The cellular damage resulting from these treatments can be monitored by Nuclear Magnetic Resonance (NMR) spectroscopy.

1.3 NMR Spectroscopy Overview

Nuclear Magnetic Resonance spectroscopy detects transitions in the magnetic energy of atomic nuclei when they are placed in a magnetic field and irradiated with radio waves. This phenomenon occurs only for atomic nuclei with a non-zero spin quantum number, i.e., those which posses an odd mass, odd atomic number or both. The sensitivity of the NMR experiment depends on two principle factors: the isotopic abundance of the NMR-active nucleus, and its magnetogyric ratio (γ). The latter (γ) is a

Reproduced with permission of the copyright owner. Further reproduction prohibited without permission.

constant that depends on the ratio of angular precession frequency to the applied magnetic field strength, $w_x = \gamma_x B_o$ [8]. Since each particular NMR-active nucleus has a different charge and mass, each has a characteristic value of γ. Hence, the larger the magnetogyric ratio for a particular nucleus, the higher the sensitivity of that nucleus in a given NMR experiment. There are a number of different NMR active nuclei that exist, and each has a unique resonance frequency at a given applied magnetic field strength. Therefore, in a given NMR experiment, set at a specific frequency, only the resonance signals from a single isotope will be detected.

Even for a given nucleus, not all of the nuclei resonate at the same frequency. Each chemically distinct nucleus present in a sample has a particular resonance associated with it, e.g. Ethanol (CH_3CH_2OH) yields three ^1H signals. Therefore, each nucleus has a distinct resonance, and these resonance peaks are separated by a chemical shift that is indicated by the ppm value given to each. This separation exists because of the different electronic environments that surround each unique nucleus. These surrounding electrons create a distinct chemical environment, which gives rise to a predictable and measurable difference in assigned chemical shift values. The number of surrounding electrons, the presence of aromatic rings, and the presence of electronegative moieties can all affect a given chemical environment in known ways.

An important feature of NMR spectra is that the total integrated area of a particular resonance signal is directly proportional to the concentration of the particular nuclei that gave rise to it. Therefore, relative concentrations for a given sample can be determined. With a number of different NMR active nuclei available, each varying in sensitivity and natural abundance, the choice of a particular nucleus is very important.

Reproduced with permission of the copyright owner. Further reproduction prohibited without permission.

The insensitivity of NMR spectroscopy is the major disadvantage of this instrument relative to other analytical tools. For a more detailed overview of NMR principles, one can refer to the book Nuclear Magnetic Resonance Spectroscopy by Frank A. Bovey [9].

1.3.1 Cancer Research via NMR Spectroscopy

Nuclear Magnetic Resonance (NMR) has been established as a noninvasive method for studying the metabolism of intact cells, tissues, and living organisms. Experiments are now being conducted to explore biosynthetic pathways, cellular metabolic activity, and intracellular reaction rates [10]. The bulk of current NMR cancer research focuses on ^{31}P and ^{1}H spectroscopy. Hydrogen-1 is the most NMR sensitive stable isotope in terms of both its high gyromagnetic ratio and high natural abundance. Phosphorous-31 has a natural abundance of 100 %, and its relative sensitivity compared to that of ^{1}H is only 6.6×10^{-2} [10]. Therefore, the corresponding order of magnitude detection limits are 0.5 mM for ^{31}P and 0.1 mM for ^{1}H NMR [10]. For cellular metabolism, one of the most important advantages of ^{31}P NMR is that it is capable of detecting metabolites, such as adenosine triphosphate (ATP), phosphocreatine (PCr), and inorganic phosphate (P_i), which play a key role in tissue metabolism. When using liquid-phase NMR, it is important to note that highly immobilized compounds give rise to signals that are often too broad to observe and therefore, are NMR-invisible [11]. For example, phospholipids incorporated in cell membranes are NMR-invisible. If the membrane is broken down, this could result in the smaller phosphodiesters, and phosphomonoesters becoming NMR-visible. NMR-invisible molecules can yield relatively uncomplicated spectra when analyzing complex mixtures such as living cells and tissues.

Reproduced with permission of the copyright owner. Further reproduction prohibited without permission.

1.3.2 Cellular Metabolites

The knowledge of how tissues of a cancerous origin differ from normal tissues may help in understanding the underlying mechanisms of cancer. Phosphorus-31 NMR studies, examining the distribution of metabolites within human breast tumours [12], and the variance in malignant and benign [13] tissue profiles from normal [14, 15], have been shown in the literature [13-15]. Proton NMR studies of the variance between breast tumours and adjacent non-involved breast tissue have also been reported [12, 16].

Due to the complex nature of both tissues and cells, a tremendous number of metabolites are to be expected. However, NMR spectroscopy can only detect a small number of metabolites, which occur naturally in large enough concentration. Expectedly, ^{1}H NMR yields the highest number of metabolites due to its natural abundance and sensitivity. However, there has been extensive work with ^{31}P, ^{13}C, ^{23}Na, ^{39}K, and ^{19}F nuclei as well. The particular NMR experiment (^{1}H, ^{31}P, or ^{13}C) that is chosen selects the particular metabolites that can be detected, and the type of tissue or cell being examined has a direct effect on which metabolites are most abundant in the sample. Each detected metabolite can reveal information about a specific biochemical pathway or can be used in combination to reveal a better picture of what is going on within the cell.

In this summary, the metabolites that most commonly occur in ^{31}P and ^{1}H NMR experiments will be discussed. Some of the most commonly observed proton metabolites are N-acetyl aspartate (NAA), creatine (Cr)/phosphocreatine (PCr), choline (Ch)/phosphocholine (PC), lactate, and a variety of sugars and amino acids. The NAA metabolite is most commonly observed in ^{1}H spectra of normal brain tissue, and its exact function is largely unknown [17]. A large number of normal tissues contain creatine and

Reproduced with permission of the copyright owner. Further reproduction prohibited without permission.

phosphorylated creatine. Although the exact role of PCr remains under investigation, these metabolites play a major role in the energy metabolism of tissues. They act as an energy buffer by retaining constant ATP levels through the creatine kinase reaction and as an energy shuttle by diffusing from energy producing to energy utilizing sites [17]. The metabolite of choline is an essential nutrient and is metabolized in three distinct pathways: Kennedy Pathway, oxidative pathway, and acetylation pathway [18]. The last ^{1}H metabolite that will be discussed is lactate. Lactate has received a lot of attention because it is a metabolically important marker of tissue ischemia and hypoxia. The formation of lactate is usually related to a decrease in high-energy phosphates, which makes lactate a good candidate for complimentary ^{1}H and ^{31}P experiments.

Previously, it has been shown that certain metabolites can be detected by using different nuclei NMR experiments. Phosphorous-31 NMR spectra share some metabolites with proton spectra. There are many other metabolites that appear in ^{31}P spectra. A ^{31}P spectrum is basically composed of two major regions: the phosphorylated metabolites related to membranes, and high-energy metabolites [19]. There are two types of phosphorylated metabolites related to membranes that are detected [20, 21]. The first type of phospholipid-related peaks is due primarily to phosphomonoester (PME), which consists of the up-field component PC [19] and the downfield component phosphoethanolamine (PE) [19]. These metabolites are synthesized by the enzymatic activity of ethanolamine and choline kinases that catalyze the first step of phospholipid biosynthesis *in vivo*. The second type of phospholipid-related peaks consists of phosphodiester (PDE) peaks. This region is due to GPC and GPE, which are the respective products of phosphatidylethanolamine and phosphatidylcholine catabolism.

Reproduced with permission of the copyright owner. Further reproduction prohibited without permission.

The high-energy metabolite region [19] of a ^{31}P spectrum usually consists of PCr, ATP, Pi, and Uridine diphosphorous (UDP) sugars. Adenosine triphosphate (ATP) is a source of free energy for biosynthetic reactions that occur in a cellular system. There are two thermodynamically favourable reactions that ATP can undergo. The first is phosphoryl transfer to form ADP and glucose-6-phosphate (G6P), and the second reaction is hydrolysis of ATP to form ADP and P_i [22]. Therefore, the decrease or increase in the level of ATP can have a direct effect on the concentration of metabolites present in the high-energy region of a ^{31}P spectrum.

At present, there are no *in vitro* or *in vivo* biological diagnostic tests that can predict the reaction of an individual tumour to chemotherapy and radiation therapy. It has been reported [20] that NMR spectroscopy can be used to detect the alterations in cellular metabolite levels following these treatments. Therefore, it may be possible to employ this method to optimize the therapeutic protocol by testing the effects of various therapeutic agents [23]. The research undertaken in this project examined the cellular metabolite levels present in the MCF-7 human breast cancer cell line, using ^{1}H and ^{31}P NMR spectroscopy. These two types of spectroscopy were used to provide a complimentary view of the metabolites present in this cell line.

1.4 Chemotherapy Summary

The ability of NMR to detect changes in tumour metabolism and effects of treatment has been established for many years [20]. However, the use of NMR as a diagnostic tool and aid to therapy is still in the preliminary stages [24]. A preliminary ^{31}P NMR study [25] reported a chemotherapeutic response to Adriamycin in the metabolism of murine mammary 16/C adenocarcinoma. The results confirmed that quantitative

Reproduced with permission of the copyright owner. Further reproduction prohibited without permission.

differences exist between the levels of specific metabolites in different tumours before and after treatment using antineoplastic agents [25]. Another study [26] examined the effects of tamoxifen, a nonsteroidal antiestrogenic agent, on MCF-7 human breast cancer. With the use of ^{31}P NMR spectroscopy, it was found that short-term tamoxifen treatment modified the content of the phosphate metabolites, increasing the ratio of nucleoside triphosphate to inorganic phosphate [26]. These results provided new information regarding the response and the mechanism of action for tamoxifen.

Since the discovery of estrogen and progesterone receptors in breast cancer cells, a number of different research projects have been undertaken to study the potential metabolic and bioenergetic perturbations among estrogen-independent, antiestrogen sensitive, and antiestrogen resistant variants of the estrogen-dependent MCF-7 human breast cancer cell line [26-28]. One group used ^{31}P NMR to investigate the effects of 17β-estraiol and tamoxifen on a series of novel MCF-7 cells that varied in their estrogen and antiestrogen responsiveness. The results of this study [27] showed that the estrogen treatment lacked consistency with respect to the significant spectral changes in any of the cell lines. However, treatment with tamoxifen showed an increase of 30-40% above the baseline for all ^{31}P spectral resonances in the estrogen-independent and -responsive cell lines. In another project [28], the effects of antimitotic drugs on a number of human breast cancer cell line variants were examined by ^{31}P NMR. These cell lines included cells that were at different stages of progression from hormone-sensitive to -insensitive as well as metastatic phenotypes. The significant differences between the spectra for the different cell lines yielded a unique marker of the metabolic state for a given cell line. The MB231 (human breast cancer) cell line was treated with a number of antimicrotubule

Reproduced with permission of the copyright owner. Further reproduction prohibited without permission.

drugs: paclitaxel, nocodazole, vincristine, and colchicines. This specific cell line was also treated with Adriamycin and methotrexate, which are non-antimicrotubule-active drugs. It was shown that antimicrotubule drugs enhanced the concentration of intracellular glycerophosphorylcholine (GPC) (relative to β-ATP). This effect was not reported for the non-antimicrotubule-active drugs [28]. To confirm the origin of the changes in GPC, a control experiment was performed. The spectra revealed that the increase in GPC was due to an increase in GPC content and not to a change in GPC relaxation times. This study demonstrated that ^{31}P NMR spectroscopy may be used as an identification tool for the various stages of tumour progression and for the prediction of anticancer treatment success [28].

It remains difficult to predict precisely which patients will initially respond to a specific therapy. A contributing factor to this, known as drug resistance, is a major clinical problem in cancer chemotherapy [29]. This occurs when a tumour is resistant to a particular drug that is being used for treatment. Another phenomenon is pleiotropic drug resistance (PDR), otherwise known as multidrug-resistance (MDR); it is manifested as a resistance to a variety of drugs with different structures and different mechanisms of action [29]. Two ^{31}P NMR studies [29-30] were undertaken to investigate the possible metabolic basis for PDR. For these studies, two types of cell lines were chosen. One was an established human breast cancer cell line (MCF-7), and the other was selected because of its PDR behaviour, plus its resistance to Adriamycin. The results showed that there were clear distinctions between ^{31}P spectra of the WT (drug-sensitive) cell line and the ADR (drug-resistant) cell line. Another study [31] employed both ^{31}P and ^{1}H NMR spectroscopy to analyze drug-sensitive (WT) and multidrug-resistant (ADR) MCF-7

Reproduced with permission of the copyright owner. Further reproduction prohibited without permission.

human breast cancer cell lines. The ^{31}P and ^{1}H NMR spectra showed differences between the WT and ADR cell lines. A quantitative comparison of the relative concentrations of the major metabolites and precursors for both types of nuclei was performed [31]. The concentrations of choline (Ch) and creatine (Cr) were calculated by subtracting their corresponding phosphorylated ^{31}P signal values from the values obtained from ^{1}H NMR spectra. The calculated choline levels for both types of cell lines are very similar. However, the calculated creatine levels show that ADR cells make more than twice as much creatine as WT cells which generate more precursors for ATP and ADP high-energy phosphorus compounds. The ability to discern the concentrations of choline and creatine provided information regarding the differences in the control of energy and phospholipid metabolism in ADR (drug-resistant) cells compared to WT (drug-sensitive) cells.

A particular type of tumour that has an inherently high resistance to conventional chemotherapy is pancreatic cancer [32]. The effects of the metabolic inhibitors on human pancreatic cancer cells using ^{31}P, ^{1}H, and ^{23}Na NMR were evaluated in the literature [32]. It was found [32] that the metabolic inhibitor 2-deoxy-D-glucose (2-DG) had similar effects on pancreatic cancer cells as on multidrug-resistant MCF-7 cells, and its cytotoxicity was much higher in these cells than in the drug-sensitive cells. Another study [33] used NMR to detect the bioenergetic changes induced in Ehrlich ascites tumour cells by the metabolic inhibitor 2-DG. It was found that when 2-DG was administered along with 3-O-methyl-D-glucose (3-O-MG) or Photosan II, there was a reduction in energy status. The post-recovery was lower with the use of the multi-drug treatment compared to the effects when either drug was administered separately. Therefore, since the metabolic

Reproduced with permission of the copyright owner. Further reproduction prohibited without permission.

depletion of ATP is known to inhibit the post-irradiation DNA repair processes, it is possible that these drug combinations, used as adjuvants to tumour radiotherapy, could enhance the therapeutic efficacy.

A different approach toward the understanding of drug-resistant tumours was reported in the literature [34]. In this study [34], plasmalemmal pH-gradients in xenografts of drug-sensitive and drug-resistant MCF-7 human breast carcinoma cells were measured by ^{31}P NMR. The use of NMR to measure intracellular pH (pH_i) is possible by examining the chemical shift of endogenous inorganic phosphate [35]. It is also possible to measure extracellular pH (pH_e) by using exogenous 3-aminopropylphosphonate (3-APP) [36]. It was found [34], for all cell lines, that the pH_e and pH_i values decreased with increasing tumour growth. However, a pH_e-pH_i gradient was found to increase with tumour size for the drug-resistant variants of MCF-7 cells but not for tumours of the drug-sensitive cells. The results state that a large pH gradient could protect the cell from weak-base drugs such as anthracyclines and Vinca alkaloids, which have pK_a values of 7.5 to 9.5. Therefore, the enhancement of the therapeutic efficacy of weak-base drugs, via metabolic manipulation of the extracellular pH, could be a possibility.

It has been shown that ^{31}P and ^{1}H NMR have the ability to detect changes in the metabolite levels induced by chemotherapy treatment. However, there is very little information in the literature that quantifies the relationship between the changes in metabolites in direct relation to the dose of chemotherapy delivered. Therefore, it is unclear whether the response of the cellular metabolites can confirm the degree of effectiveness for a given chemotherapy treatment.

Reproduced with permission of the copyright owner. Further reproduction prohibited without permission.

1.5 Radiation Therapy Summary

Differences between the NMR spectra of normal and tumour cells could lead to new methods of radiation treatment. These treatments would be directed toward differentially enhancing the manifestations of radiation-induced damage in tumours and minimizing damage in normal tissues. This would ultimately improve the efficacy of tumour therapy [37]. In the literature, one group [37] used ^{31}P NMR to study the effects of radiation treatment on Ehrlich ascites tumours, which were treated with 2-DG and Photosan-3. It was found that the combination of these two drugs had the potential to be used as an adjuvant to tumour radiotherapy. The same conclusion was reported in an earlier study [33], which used the Ehrlich ascites cell line. Therefore, the results of these studies [37] add to the validity of these drugs potentially being used in therapeutic practices. In a different study [38], ^{31}P and ^{1}H NMR were employed to examine the effects of brain tumour radiotherapy. The purpose of this study was to monitor the changes that occur in the human brain following fractionated clinical radiotherapy. This is important because external beam radiation treatment of brain tumours results in radiation exposure of normal tissue that lies within the treatment area. This can cause delayed effects such as demyelination and radiation necrosis. The results of this study [38] suggest that any radiation-induced damage that may occur from brain tumour treatment is invisible to ^{31}P NMR spectroscopy. However, ^{1}H spectra did show post-irradiation changes in the ratios of Ch/NAA, Cr/Ch, and NAA/Cr [42]. In a more recent study, it was confirmed that ^{1}H NMR could detect the metabolic effects of radiation treatment on brain tumours [39]. This study [39] specifically looked at monitoring the changes that occurred during post-surgical fractionated radiotherapy [39]. It was shown

Reproduced with permission of the copyright owner. Further reproduction prohibited without permission.

that in order to establish biological markers for radiation damage in the treatment of brain tumours an analysis of all visible metabolites, as opposed to the use of just specific ratios, is required [39]. Similarly, using an analysis of correlation between measured parameters, a ^{31}P NMR study [40] looked at the acute effects of γ-radiation on rat brain metabolism. This study reported changes in the relative levels of brain phosphate metabolites and intracellular pH at selected times post-irradiation corresponding to a single dose of 6.5 or 300 Gy. Phosphorous spectra showed only minor changes post-irradiation. A new parameter called the Z-index was used for spectral analysis. The Z-index is a mathematical manipulation of the integral intensities of each peak found in the ^{31}P spectra and includes the intracellular pH value. For each animal, these variables were normalized to the total NMR-visible phosphate content. The Z-index, a multi-dimensional statistical analysis, has the ability to correlate changes in a number of parameters that characterize the system as a whole [40]. The results showed an increase in Z value one day after 300 Gy was administered and two days after a lower dose of 6.5 Gy was used. Due to the fact that only minor changes were reported for integral values [40], the Z-index may be a more sensitive indicator of an imbalance in brain energy metabolism.

As shown previously [29], a major clinical problem in chemotherapy is drug-resistance. Similarity, it has been reported repeatedly [41-45] that different types of tumours can display varying radioresistant and radiosensitive responses towards radiation treatment. In radiation therapy, tumour oxygen content is considered a strong biological modifier of ionizing radiation effects [46]. The absence of oxygen is believed to interfere with the intracellular biochemical events following irradiation [4], and the degree of

Reproduced with permission of the copyright owner. Further reproduction prohibited without permission.

sensitization to oxygen is described by the oxygen enhancement ratio [4]. The oxygen enhancement ratio is defined as the ratio of doses necessary to achieve the same biological effect in the presence or absence of oxygen [4]. Therefore, tumour hypoxia has been considered a major cause of cellular necrosis and radiation failure [47]. To explore this effect by using NMR, a study [48] of the changes in ^{31}P spectra of irradiated radioresistant mammary carcinoma (MCa) and radiosensitive methylcholanthrene-induced fibrosarcoma (Meth-A) tumours was performed. These two tumour models were chosen because both differ in radiosensitivity due to their inherent oxygenation states. The ^{31}P spectra showed differences in the metabolites of these two tumour models, particularly in the PCr/Pi ratio. It was concluded that the metabolic differences observed in this study were related to variations in tumour perfusion and energy metabolism. Nevertheless, this study indicates that it may be feasible to relate differences in the tumour radiosensitivity of ^{31}P spectra obtained non-invasively. A more recent study [49] used ^{31}P NMR spectroscopy to examine the effects of radiation treatment upon a hypoxic murine mammary carcinoma. The tumors were monitored over the course of nine days, starting prior to irradiation and continuing post-irradiation. The tumours were irradiated with a single dose of 0, 4, 8, or 17 Gy, and the results were then combined with the results from a previous study [50] performed by the same research group, which used a single dose of 32 and 65 Gy on the same tumour model. The results showed changes in tumour metabolism post-irradiation that include a dose-dependent change in the relative amounts of phosphomonoesters, an increase in the PCr/Pi and NTP/Pi ratios, and an increase in one of the PDE peak components, GPC, relative to β-NTP (nucleotide triphosphate). This study reported that both dose and time post-irradiation have

Reproduced with permission of the copyright owner. Further reproduction prohibited without permission.

significant effects on phosphorus metabolite analysis. However, the feasibility of a dose-response relationship was confirmed in a different study [51]. This group used ^{31}P NMR spectroscopy to evaluate the effects of radiation on L 1210 cells. The results indicated a relationship between the applied radiation dose and the measurement of ATP concentration. This trend is not seen for all types of cell lines or tumours. A study [52] of the effects of radiation on phosphorus metabolites in two well-established human squamous cell carcinoma (SCC) cell lines (SQ38 and SQ20B) [53, 54] was performed. These two cell lines are known to have different radio sensitivities. The results showed that statistically all measured metabolite levels (energy metabolites and membrane metabolites) had insignificant changes with respect to their controls. Therefore, one can see that further NMR studies are required in order to determine if this dose-dependent correlation can be utilized as a potential therapeutic tool.

A number of ^{31}P NMR spectroscopy studies have explored the mechanism of radiation-induced damage by examining the gain and loss of ATP signal intensities [51, 55, 56]. These intensities were determined by measuring the ATP:ADP:Pi phosphate signals. However, a number of studies [21, 57-62] have shown that the phospholipid turnover parameter is a possible biomarker for radiation-induced responses in both *in vivo* and *in vitro* experiments. A ^{31}P NMR study was undertaken [21] that examined the radiation response of Ehrlich ascites tumour cells following a dose of 6 Gy. The reasoning for this study [21] was to identify possible biomarkers of radiation response. The results showed a continuous decrease in the amount of PME and PDE up to 2 hours post-irradiation. In addition, the PC/GPC ratio in irradiated cells showed a large decrease, compared to the untreated cells, at the time interval of 3-7 hours post-irradiation. This

Reproduced with permission of the copyright owner. Further reproduction prohibited without permission.

further confirmed past reports [57, 58] that showed the PME peak as a sensitive indicator of post-irradiation tumour cell response. In previous studies of Non-Hodgkin lymphoma [59] and murine mammary carcinoma NU-82 [60], it was reported that the PDE region has the most radiation sensitive metabolites, making this region a possible pathological marker in steady-state response. In a different ^{31}P NMR study [61], the effects of radiation on phospholipid-related peaks in mammary carcinoma tumour extractions were explored. It was reported [61] that 24 hours after a dose of 32 Gy was delivered, there was a significant increase in the ratio of PE/PC, and the ratio of ethanolamine-containing to choline-containing phospholipid metabolites showed a large increase between 48 to 96 hours post-irradiation. Similar results were seen in the spectra of a single dose of 65 Gy. It was concluded [61] that the post-irradiation response of the lipids occurred more slowly when compared to the metabolites, and therefore, the changes in the phospholipids are secondary to the changes in the metabolites. It should also be noted that distinct changes in phospholipids became visible only 48 hours post-irradiation [61]. In another ^{31}P NMR study, the post-irradiation effects on radiation-induced fibrosarcoma-1 (RIF-1) tumour model were examined over the course of seven days [62]. The results showed that the two primary changes in ^{31}P NMR spectra are the increase in PME/PC and in GPC/NTP ratios that were reported to occur directly at the cellular level [62]. From these studies [57-62], it can be concluded that the phospholipid profiles of tumour cells can represent a reliable and sensitive biomarker for the assessment and monitoring of radiation response. These studies [57-62] do not provide a quantitative method, which would allow the change in phospholipid metabolite profiles to be used as a tool to predict

Reproduced with permission of the copyright owner. Further reproduction prohibited without permission.

post-irradiation dose effects. Hence, there is only a distinct qualitative response in phospholipid metabolites post-irradiation for the examined tumour and cell types [57-62].

The accumulation of data formulated from the previous studies [37-64] has indicated that NMR has the ability to indirectly monitor induced changes in cellular metabolites. A study [65] that explores the possibility of using ^{31}P NMR to predict the optimum interval between fractionated irradiation doses has been reported. This study [65] reported changes in the metabolites of murine mammary carcinoma (FM3A) cells in a fractionated experiment. The radiation was delivered using two fractions at a dose of 5 Gy per fraction, and the radiation was given at 0, 1, 2, 3, and 6-day intervals [65]. The mean β-ATP/P_i and PCr/P_i ratios on day two post-irradiation were significantly higher than the pre-irradiated levels. After day two, these ratios decreased sharply and returned to the initial ratio values on day three. The results showed that fractionated irradiation, with a 2-day interval, had more of an effect on β-ATP/P_i and PCr/ P_i peak ratios than other fractionated schedules. Assays were then performed on the irradiated samples to determine the growth fraction of the samples. It was found [65] that the maximum growth fraction occurred at two days post-irradiation, which coincided with the results for fractionation. It was concluded [65] that β-ATP/P_i and PCr/ P_i peak ratios could be a potential indicator for determining the fractionation schedule in radiation therapy.

The use of ^{1}H NMR, in comparison to ^{31}P NMR, yields spectra that consist of more peaks, which are due to the increased sensitivity of the proton nuclei and the natural abundance of proton metabolites [10]. Through the use of ^{1}H NMR [55, 63, 64], it has been shown that lactate could serve as a sensitive biomarker of tumour response. An early study [55] that looked at Ehrlich ascites tumour cells, reported that changes in

Reproduced with permission of the copyright owner. Further reproduction prohibited without permission.

lactate production were found, with a marked increase occurring 24 hours post-irradiation. These findings were further supported by another study [63] that detected a substantial decrease in the lactate/creatine and lactate/choline values in the D-54 MG cell line post-irradiation. More recently [64], the effects of γ-radiation on the lactate levels of EMT6 tumours were reported using ^{1}H NMR. This study monitored EMT6 tumours over the course of two days. The first spectrum was taken pretreatment, and additional spectra were taken at 24 and 48 hours after irradiation doses of 4, 10, or 20 Gy were administered. The results showed [64] a 21% decrease in the lactate level at 48 hours after an irradiation dose of 10 Gy, and a 40% decrease was observed at 48 hours after an irradiation dose of 20 Gy. These studies [55, 63, 64] showed that the largest change in proton spectra post-irradiation is the decrease in lactate resonance, which could be used as a biomarker in tumour response.

1.6 Cellular Metabolite Extraction Summary

Previous work [66] has indicated that the signal resolution in cellular extracts is increased compared to that of *in vivo* systems. This result is due to the increased mobility of metabolites in a non-viscous environment [67]. Another major factor contributing to the increase in signal resolution in cellular extracts is the ability to provide greater concentrations of cellular metabolites in the fixed volume used for NMR. Therefore, cellular extraction was used for this research in order to examine the cellular metabolite levels in their most NMR-sensitive state. A number of different types of cellular extraction procedures have been used in the preparation of cells for NMR studies. Studies have shown that a Dual-Phase Extraction (DPE) [68, 18] method has been developed. This method extracts both the water-soluble and lipid metabolites from the same sample

Reproduced with permission of the copyright owner. Further reproduction prohibited without permission.

at the same time. However, the two most widely used extraction methods are the Perchloric Acid Extract (PCA) method and Folch's method of extraction.

Folch's method is used for the extraction of cellular lipid metabolites. Folch *et al.* [69] first proposed this method in 1957. More recently, Folch's original method of extraction has been slightly modified for the extraction of cellular lipids in cell cultures [15, 70]. The first step in this procedure was to wash the cell culture plates with a saline solution at room temperature. The next step was to add ice-cold methanol to each plate, and then place the plates on ice for 5 to 10 minutes while a rubber policeman was used to scrape the cells into pools. At this point, two volumes of chloroform were added and mixed, followed by 0.6 volume of 0.1M KCl. The samples were vigorously mixed and left overnight at 4 ℃ in order to allow for phase separation. The lipids were obtained from the bottom layer. The final step of this method of extraction was to dissolve the lyophilized sample in the solvent of choice for the NMR experiment.

The PCA extraction method is used for the extraction of water-soluble cellular metabolites. There are a number of different modified PCA extraction methods [71-74] available. All of these methods follow a general experiment scheme. The first step in the PCA extraction was to harvest the cells from the culture plates using a reagent such as a Trypsin-EDTA solution. Once the cells were collected and washed, they were subjected to ice-cold Perchloric acid (0.5 M) in a volume that is dependent upon the number of cells initially used. Following the addition of perchloric acid, the mixture was sonicated for 5 minutes at a temperature of 4 ℃. The solution was neutralized, using 5M sodium hydroxide, and then centrifuged to remove the potassium perchlorate precipitate. The supernatant was treated with Chelex 100, and then the solution was adjusted to a pH of ~

Reproduced with permission of the copyright owner. Further reproduction prohibited without permission.

8. This solution was lyophilized and then stored at -20 ℃ or colder in order to prevent hydrolysis. The final step in this method of extraction was to dissolve the lyophilized sample in the solvent of choice for the NMR experiment.

1.7 Thesis Objective

This research project performed a feasibility study to quantify the effect of radiation therapy on the cellular metabolite levels of the MCF-7 cancer cell line. The effects of radiation therapy were examined by ^{31}P and ^{1}H NMR spectroscopy. The most important step in this quantitative study was to establish the limitations in the reproducibility of NMR spectra for a cellular system. Due to reported variations [15, 55, 68, 70] in NMR spectra of cellular metabolites in various samples of non-treated cells, it can be noted that a minimum deviation exists pre-irradiation. Hence, the deviation seen in the spectra of non-treated cells must be minimized and quantified before the effects of irradiation on cellular metabolites can be quantified.

Reproduced with permission of the copyright owner. Further reproduction prohibited without permission.

2.0 EXPERIMENTAL:

2.1 Nuclear Magnetic Resonance Spectroscopy

All proton (^{1}H) and phosphorous (^{31}P) nuclear magnetic spectra of MCF-7 cancer cells, a commercially available human breast cancer cell line, were acquired using a Varian UNITY Inova 500 NMR spectrometer system. This spectrometer operates on a Sun Ultra 5 Workstation. Both proton and phosphorous nuclei were measured in a 5 mm probe, which was set at a temperature of 23°C and at operating frequency of 499.72 MHz and 202.29 MHz, respectively.

	Recycle Delay	Pulse	Acquisition Time	Data Points /FID	Sweep Width	Number of Transients
^{1}H	1.0 sec	9.2 μsec 90° spin-angle flip	1.67 sec	26, 668	8, 000	100
^{31}P	2.0 sec	9.5 μsec 90° spin-angle flip	1.0 sec	16, 000	8, 000	800

Table 1. Acquisition parameters used for ^{1}H and ^{31}P spectra.

Proton spectra were acquired using the presaturation technique to suppress the residual water signal contained in the extracted samples. The saturation delay and saturation power were maximized in order to optimize the presaturation technique in the samples. Through trial and error, the values were set at 5.0 s for a saturation delay, and the saturation power was set to 22. The acquisition parameters listed in Table 1 yielded ^{1}H spectra with reasonable signal-to-noise (S/N) ratio in less than 15 min.

Phosphorous spectra were acquired using gated proton broadband decoupling to eliminate ^{1}H-^{31}P NMR multiplets as well as nuclear Overhauser enhancement artifacts. Under these conditions, each spectral resonance corresponds to a distinct phosphorous

Reproduced with permission of the copyright owner. Further reproduction prohibited without permission.

spin site. The acquisition parameters yielded ^{31}P NMR spectra with reasonable S/N in less than 45 min (Table 1). Phosphorous spectra were Fourier-transformed using 6 Hz exponential multiplication, phased, and referenced to internal inorganic phosphate peak (set to 1.8 ppm).

2.2 Cell Culture

A human breast carcinoma cell line, known as MCF-7, was used for all cell extraction experiments. This cell line was cultured in tissue culture dishes (15 cm in diameter) using Dulbecco's modified Eagle's medium (DMEM), which is supplemented with 10% fetal bovine serum, 4500 mg glucose/L, L-glutamine, $NaHCO_3$, streptomycin (100 μg/mL), amphotericin (0.25 μg/mL), and 60 units/mL of penicillin. The tissue culture dishes were stored in an incubator at 37 ℃ under a 5% carbon dioxide/air atmosphere.

2.3 Irradiation Procedure

The cell culture dishes, including control dishes, were removed from the incubator, and brought to the Siemens Oncor accelerator. A 20 x 20 electron applicator was fixed to the head of the accelerator, and the cells were placed on the table at 100 cm SSD (source to surface distance). The energy used was 6 MeV with approximately 2 mm build up. After the specified amount of irradiation was delivered to the cell dishes, they were immediately returned to the incubator along with the control dishes. At this point, the cell culture dishes remained in the incubator for a determined length of time, post-irradiation, and then underwent a freeze-thaw extraction procedure.

Reproduced with permission of the copyright owner. Further reproduction prohibited without permission.

2.4 Freeze-Thaw Extraction

The DMEM was removed for the cell culture dishes (3 dishes per sample) and then the dishes were washed with phosphate buffer saline solution (PBS) at room temperature. The dishes were aspirated and a Trypsin-EDTA solution was added and left for 2-3 min until the cells visually detached from the culture dishes. This suspension, which contained the MCF-7 cells, was transferred into a 50 mL conical tube. The culture plates were washed with additional DMEM to collect any cells that might have been left behind, and this solution was then added to the conical tube. The conical tube was placed into a GS-GKR Beckman Centrifuge at room temperature for 5 continuous min at 1100 rpm. The supernatant, which contained a mixture of DMEM and Trypsin-EDTA, was aspirated, and the cells were washed with balanced salt solution (BSS) that contained no phosphorous. The conical tube was placed back into the centrifuge for 5 min. The supernatant was aspirated, and the cells were washed with BSS again. The conical tube was placed back into the centrifuge for 5 min. The supernatant was decanted, and the cells were re-suspended in deuterium oxide (D_2O), which was transferred evenly into a number of 1 dram glass vials. These vials were placed into a SANYO ultra low freezer at –84 ℃ for one hour, and then transported (~ 30 min.) to Lakehead University using a Thermos flask containing dry ice. The vials were removed from the dry ice and placed on the bench top for 5 min without their caps (to prevent the vials from exploding). They were then re-capped and placed into a room temperature water bath for 15 min. The cellular suspension contained in each vial was transferred into a 1.5 mL Eppendorf microcentrifuge tube and sonicated on ice for 10 s using a 20 kHz, 350 W Branson Sonic Power probe sonicator with the output control set at 4. After centrifugation at 11,000 rpm

Reproduced with permission of the copyright owner. Further reproduction prohibited without permission.

for 2 min, the supernatants were decanted into glass-weighing bottles, and frozen in a liquid nitrogen/ethanol bath. The samples were transferred directly to a Labconco Freeze Dry System and lyophilized at –30 ℃ and 250 mbar for 24 h. After the completion of freeze-drying, only one sample at a time was removed. The remaining samples were left in the freeze dryer at a temperature of -30 ℃ to protect against hydrolysis. Each freeze-dried sample was transferred to a 1.5 mL microcentrifuge tube and resuspended in 1 mL D_20 containing 0.63 M $MgCl_2$. Finally, the sample was sonicated on ice for 10 s and transferred to 5 mm diameter NMR tube. It was concluded that a 10 mm diameter tube was not optimal due to sample concentration requirements.

Reproduced with permission of the copyright owner. Further reproduction prohibited without permission.

3.0 RESULTS AND DISCUSSION:

3.1 Extraction Procedure

The first step in this research project was to determine which cell line would be used for metabolite analysis. Two possible cell lines were evaluated: a human breast cancer cell line 'MCF-7' and a human ovarian cancer cell line 'OVCAR'. Whereas ^{31}P NMR spectra of OVCAR are dominated by a single metabolite signal (Figure 1.A), the MCF-7 cell line yielded a number of ^{31}P metabolite signals (Figure 1.B) and was thus chosen for further analysis.

A series of changes in the handling of the cell samples were implemented in order to improve the reproducibility of the control samples.

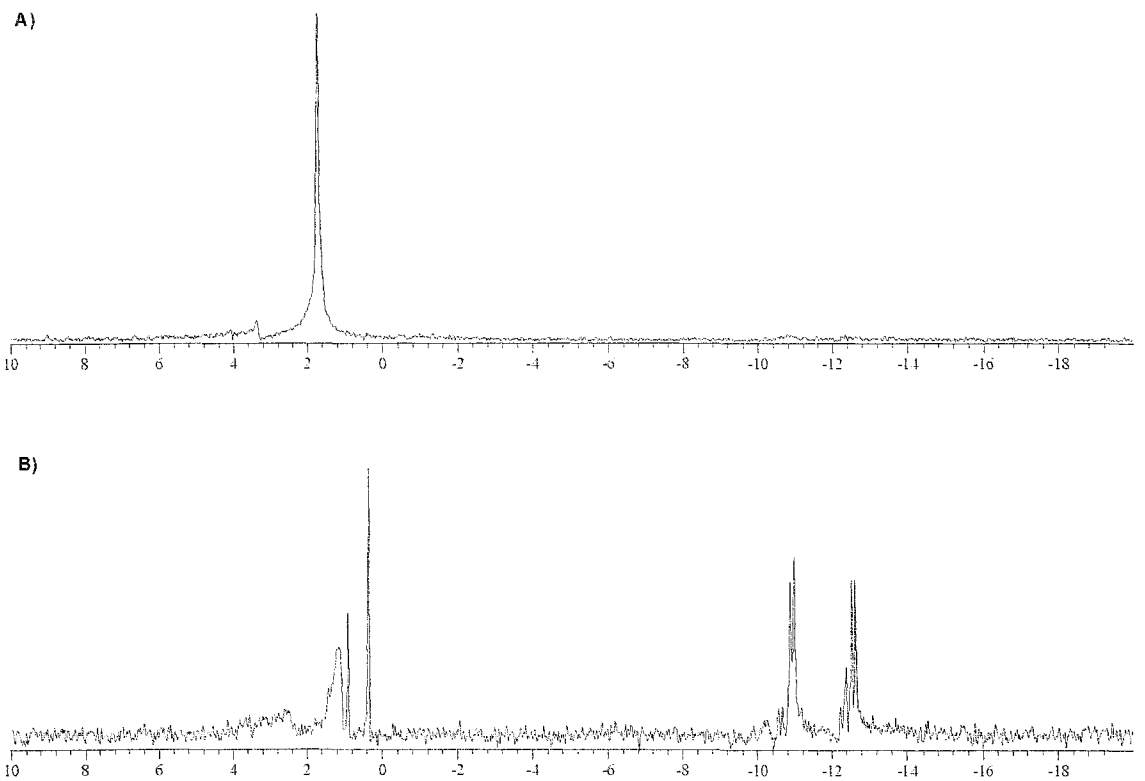

Figure 1. A, ^{31}P spectra of intact cells for the OVCAR cell line; B, ^{31}P spectra of intact cells for the MCF-7 cell line.

Reproduced with permission of the copyright owner. Further reproduction prohibited without permission.

These changes optimized parameters such as temporal stability, ^{31}P signal-to-noise ratio, inter-batch reproducibility, and intra-batch reproducibility. The modifications to the cell handling and extraction procedures are presented here in chronological order. Once the MCF-7 cells were removed from their culture dishes, the new unstable environment conceded a slow onset of cellular death causing large variations in ^{31}P spectra. This existed even when the samples were acquired at a specific time post removal. Cellular fixation using both para-formaldehyde and ethanol was attempted [75]. Unfortunately, when the para-formaldehyde fixative was employed, the resulting ^{31}P spectra were dominated by the inorganic phosphate signal (Figure 2.A). When the ethanol fixative was used, the signal-to-noise (S/N) ratio was greatly decreased (Figure 2.B).

Instead, it was decided that the MCF-7 cells would be suspended in a number of different solvents. The solvents that were chosen are distilled de-ionized water (DDW)/25% D_2O, balanced salt solution (BSS)/25% D_2O, and 100 % D_2O. The use of different solvents yielded poor spectral reproducibility. The solvents had varying effects on not only the S/N ratio in the ^{31}P spectra, but also on the relative peak heights of metabolite signals that were present (Figure 3). These results were attributed to the manner in which these solvents directly affected the MCF-7 cells in suspension. The BSS solvent keeps the cells intact, while a large number of the cells suspended in DDW/25% D_2O solvent are lyzed. This hypotonic solvent creates osmotic pressure due to the migration of water into the MCF-7 cells, which causes the cells to rupture. This process releases the phosphorus metabolites into solution, resulting in a greater S/N ratio for ^{31}P spectra (Figure 3) due to the increased mobility these metabolites have in the less viscous environment. This has been well documented the literature [67].

Reproduced with permission of the copyright owner. Further reproduction prohibited without permission.

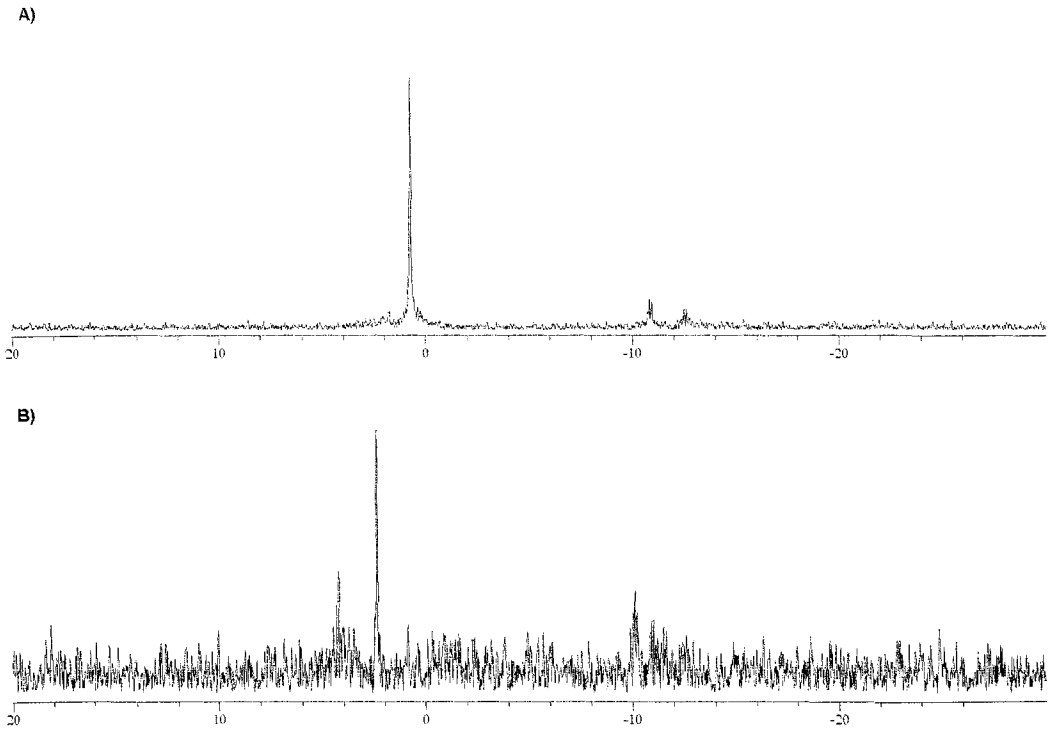

Figure 2. A. ^{31}P spectra of MCF-7 cells fixed using para-formaldehyde; B. ^{31}P spectra of MCF-7 cells fixed using ethanol.

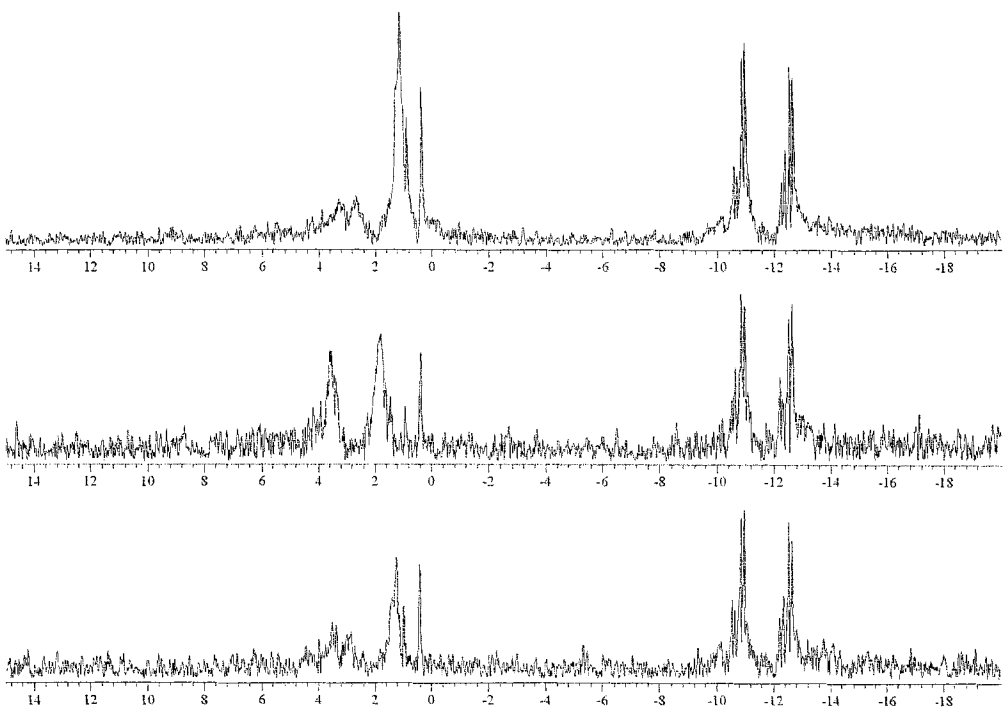

Figure 3. ^{31}P spectra of MCF-7 cells suspended in different solvents; DDW/25% D_2O (Top), BSS/25% D_2O (middle), and 100% D_2O (Bottom).

Reproduced with permission of the copyright owner. Further reproduction prohibited without permission.

At this point in the extraction procedure, the solvent of DDW/25% D_2O was chosen because of its increase in S/N ratio. It has been reported [79] that the divalent metal ion Mg^{+2} assists in the stabilization of high-energy phosphate metabolites. Therefore, a number of ATP control standards that contained varying concentrations of $MgCl_2$ were prepared. It was found that the concentration (0.63 mol/L) of $MgCl_2$ yielded the highest increase in the consistency between metabolite ratios. There was also a slight increase in the average percent error for all the relative metabolite peak ratios found in ^{31}P spectra (Table 2 and Table 3). The resonance signals were broadened for the magnesium samples, resulting in only three singlet peaks, which is in agreement with published results [77]. However, the loss in resolution was accepted for the gain in overall reproducibility. Therefore, this concentration of Mg^{+2} was added to the DDW/25% D2O solvent, and the results showed a qualitative improvement in reproducibility (Figure 4).

Ratio	β-ATP(2) /γ-ATP(1)	β-ATP(2) /γ-ATP(2)	β-ATP(2) /α-ATP(1)	β-ATP(2) /α-ATP(2)	β-ATP(2) /β-ATP(1)	β-ATP(2) /β-ATP(3)
SD	0.01167	0.00149	0.00193	0.00487	0.00674	0.00674
Percent	0.146	0.179	0.278	0.328	0.326	0.435

Table 2. Standard deviations (SD) for NMR experiments (n=3) performed on a single ATP DDW control sample, and the percent difference compared to the average value of the four runs for each ratio. The four spectra were acquired at 30 min after the preparation of the sample.

Ratio	β-ATP/γ-ATP	β-ATP/α-ATP
SD	0.00247	0.00247
Percent	0.247	0.247

Table 3. Standard deviations (SD) for NMR experiments (n=3) performed on a single ATP DDW/Mg^{+2} [0.63 M] control sample and the percent difference compared to the average value of the four runs for each ratio. The four spectra were acquired at the same times post-preparation as in Table 2.

Reproduced with permission of the copyright owner. Further reproduction prohibited without permission.

Nevertheless, the spectral differences were still too large and inconsistent for quantative analysis. It was speculated that hydrolysis was still occurring due to the concentration of DDW present in the sample. An ATP control was made using D_2O (0.63 M $MgCl_2$) as the solvent. It was found that the switch to D_2O (0.63 M $MgCl_2$) had a positive effect on the control's reproducibility (Table 3). This enhancement could be explained by the isotopic effect of D_2O on hydrolysis reactions. This solvent, compared to H_2O, would decrease the reaction rate of hydrolysis.

An advantage of the D_2O (0.63 M $MgCl_2$) solvent was a large reduction in the ^1H NMR water resonance peak for this cellular suspension. With the use of the presaturation technique, it was possible to perform better ^1H NMR experiments to complement the ^{31}P NMR experiments.

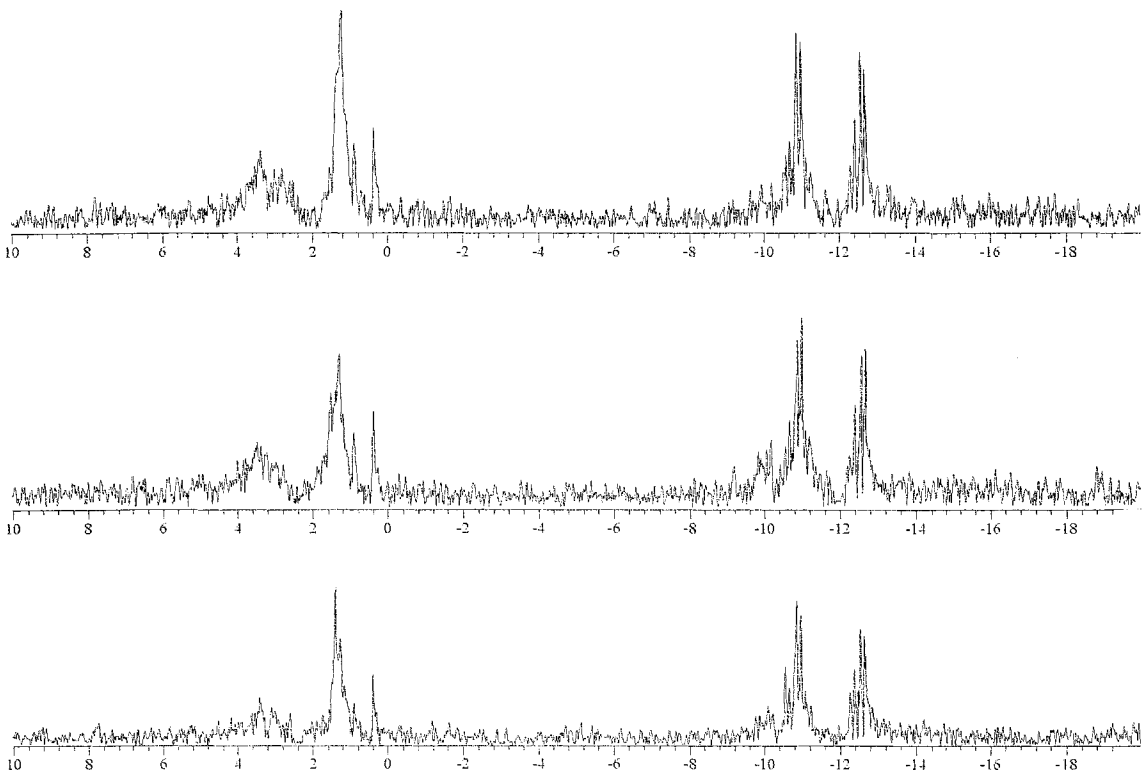

Figure 4. ^{31}P spectra of MCF-7 cells suspended in DDW Mg^{+2} [0.63 M]/25% D_2O. Each spectrum is from a different sample that underwent the identical extraction procedure.

Reproduced with permission of the copyright owner. Further reproduction prohibited without permission.

Ratio	β-ATP/γ-ATP	β-ATP/α-ATP
SD	0.00112	0.00178
Percent	0.132	0.207

Table 4. Standard deviations (SD) for NMR experiments (n=3) performed on a single ATP D_2O/Mg^{+2} [0.63 M] control sample, and the percent difference compared to the average value of the four runs for each ratio. The four spectra were acquired at the same times post-preparation as in Table 2 and Table 3.

Unfortunately, the use of D_2O as a solvent limited the S/N ratio. To compensate, sonication was employed in order to lyze the cells further while suspended in the D_2O/0.63 M $MgCl_2$ solvent (provided in Figure 5). After a number of different experiments, it was determined that sonication yielded a non-reproducible decomposition of high-energy metabolites or a non-reproducible degree of lyzing (Figures 5 and 6).

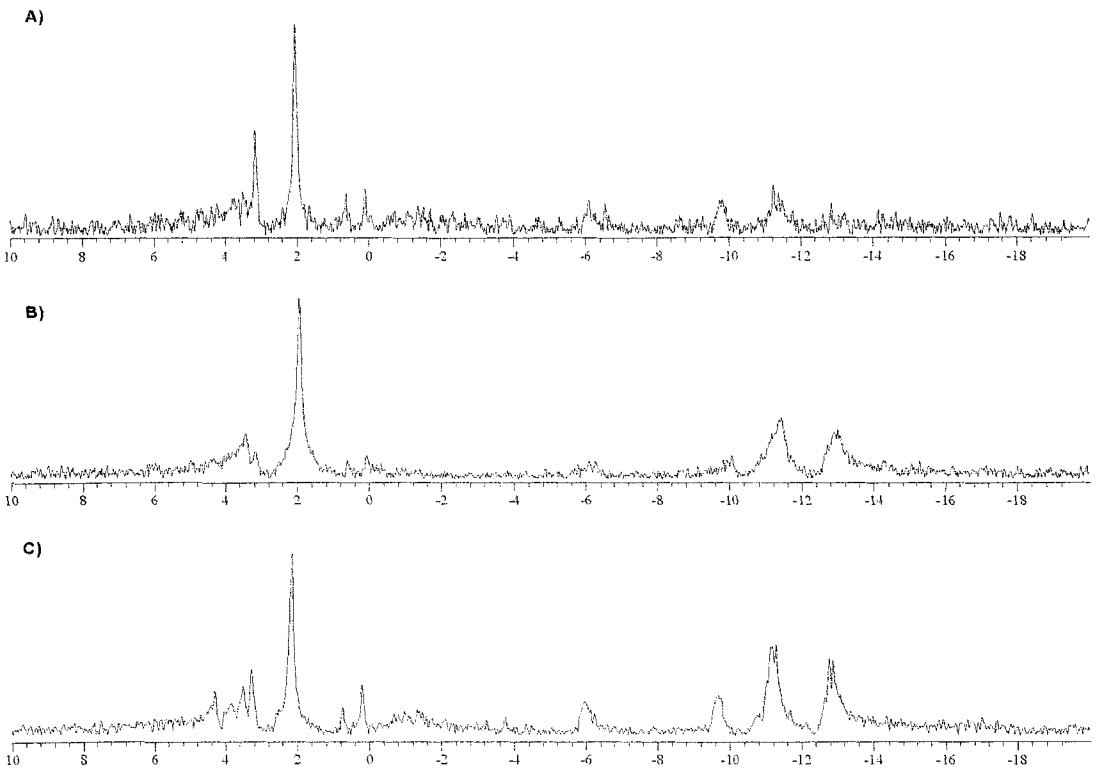

Figure 5. ^{31}P spectra that show variations due to different sonication procedures; A, output control was set to 7 and the sample was sonicated over five 10 s intervals; B, output control was set to 2 and the sample was sonicated over three 20 s intervals; C, output control was set to 6 and the sample was sonicated over four 10 s intervals.

Reproduced with permission of the copyright owner. Further reproduction prohibited without permission.

Subsequently, sonication could induce hydrogen exchange with the D_2O solvent to form the HOD peak that is shown to dominate most ^1H spectra; two examples of this are displayed in Figure 6 (B and C). The sonication process was optimized for reproducibility, and relied on three variables: output control; length of sonication; and number of sonication runs. Table 5 summarizes the experiments performed and the different sonication settings used for each. A qualitative comparison of the spectra indicated that the highest reproducibility could be achieved with an output setting of 4 and one application of 10 s (Figure 7). Centrifuging was attempted in order to remove the bulk of cellular debris, but the cellular suspension could not be separated. The disadvantage of this procedure is that samples contained a large amount of water. Hence, the pre-saturation method was not completely successful in suppressing the water resonance peak in ^1H spectra (~ 7.2 ppm) (Figure 7.B).

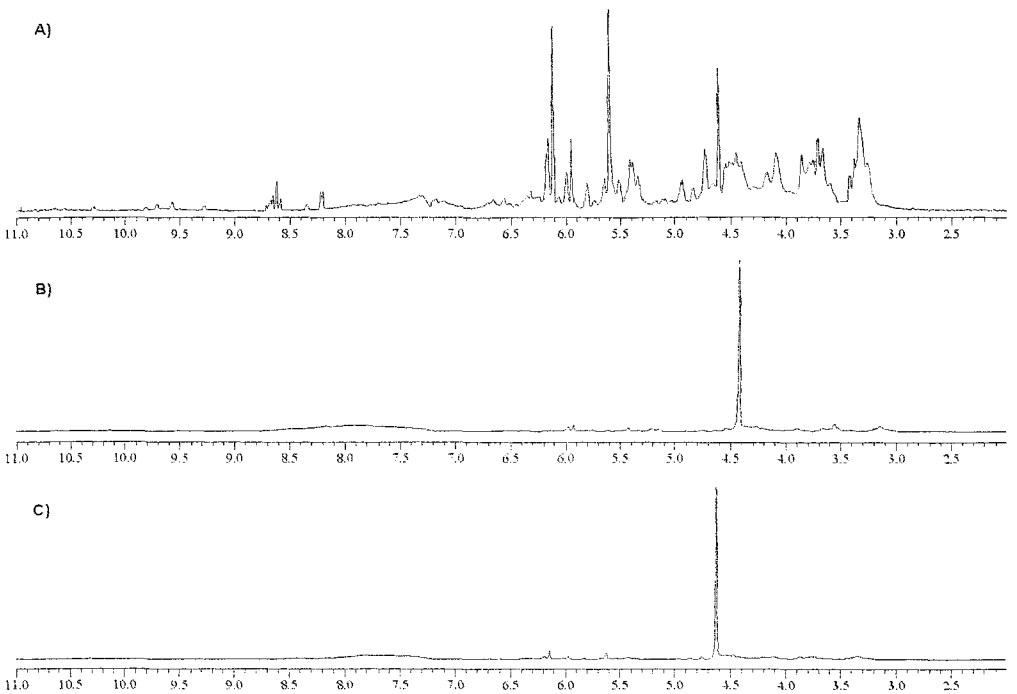

Figure 6. ^1H spectra that show variations due to different sonication procedures; A, output control was set to 7 and the sample was sonicated over five 10 s intervals; B, output control was set to 2 and the sample was sonicated over three 20 s intervals; C, output control was set to 6 and the sample was sonicated over four 10 s intervals.

Reproduced with permission of the copyright owner. Further reproduction prohibited without permission.

Output Control	Duration/s	Sonication Intervals
7	10	3
7	10	5
6	10	4
4	**10**	**1**
2	10	3
2	20	3
2	30	3

Table 5. Each row describes an experiment that was performed using an identical procedure that only varies with sonication parameters. All experiments were performed using D_2O/Mg^{2+} as the solvent and sonication was performed with the sample on ice.

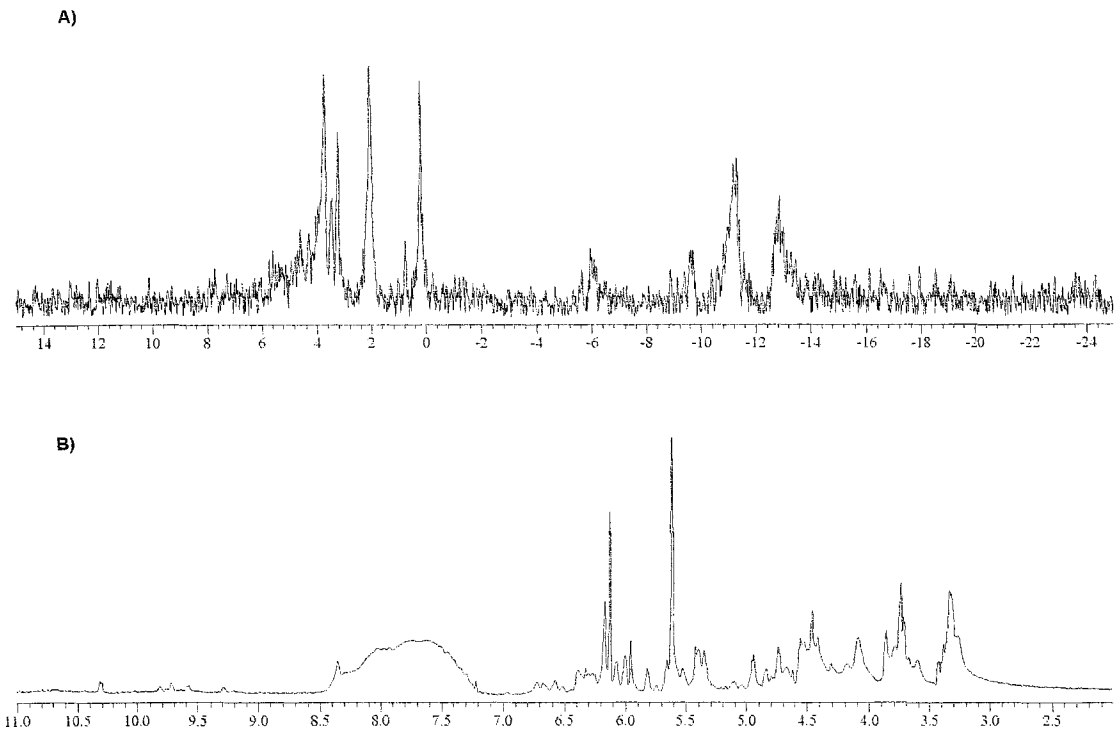

Figure 7. A, ^{31}P spectrum of the optimized sonication procedure; B, ^{1}H spectrum (using presaturation) of the optimized sonication procedure.

Reproduced with permission of the copyright owner. Further reproduction prohibited without permission.

Due to hydrolysis reactions, the internal water from the cells and the water contaminants contained within the D_2O solvent can create instabilities for the metabolites of the sample. To remove the water from the samples, a freeze dryer was used following the sonication step. The spectra resulting from the optimized sonication procedure, followed by 24 h freeze dry at –30 ℃, are shown in Figure 8. An improvement in the S/N ratio was desired before quantative analysis could be carried out. A number of different methods were attempted. The method that showed the greatest potential was "freeze-thawing". In this method, samples were pre-frozen at –84 ℃, which reportedly [79] has no affect on the cell's viability. A freeze-thaw cycle was used because the literature [78] states that the viability of cells that undergo fast freezing (70 ℃/min) and thawing is around <0.1%, and this step was introduced as the first step in the extraction procedure.

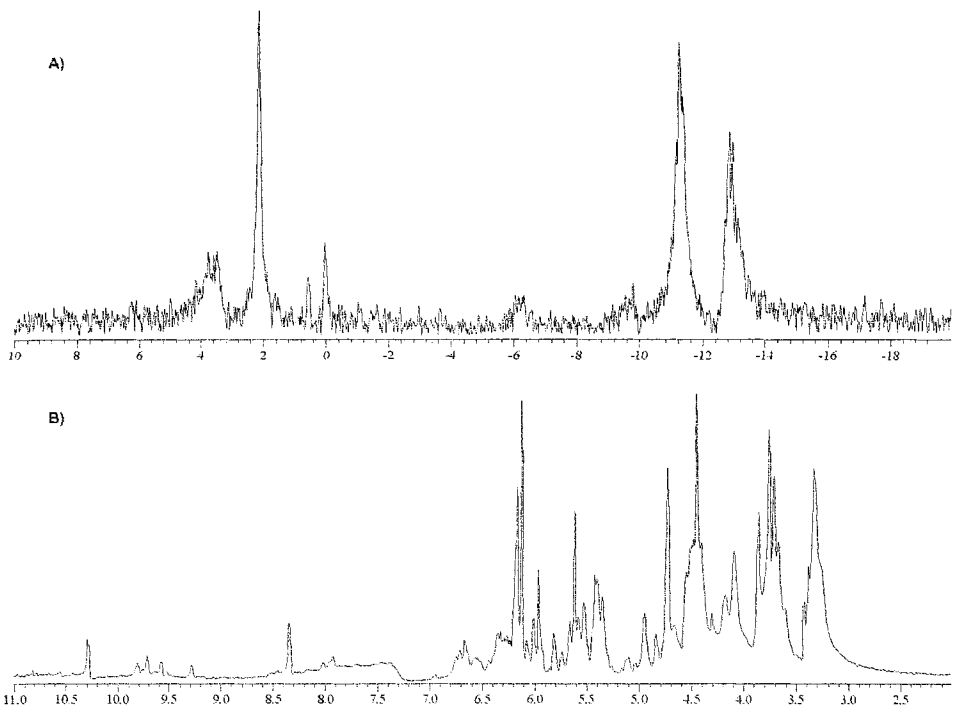

Figure 8. A, ^{31}P spectrum of an extract that underwent freeze-drying following the previously determined sonication procedure; B, ^{1}H spectrum (using presaturation) of an extract that underwent freeze-drying following the previously determined sonication procedure.

Reproduced with permission of the copyright owner. Further reproduction prohibited without permission.

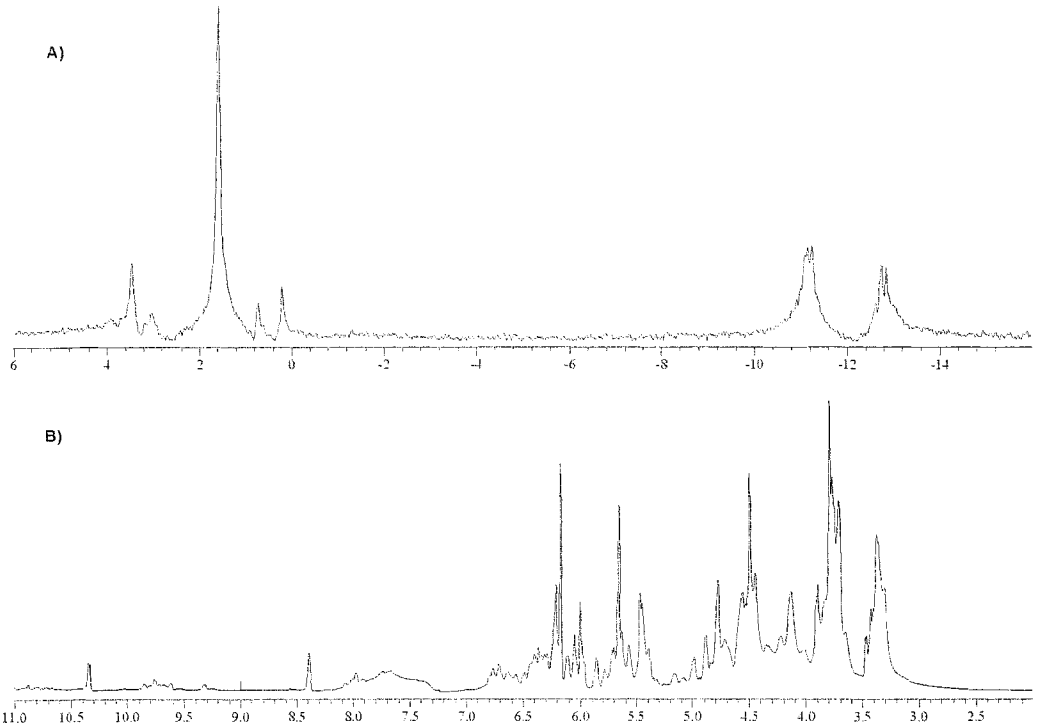

Figure 9. A. ^{31}P spectrum of an extract that underwent the finalized (freeze-thaw) extraction procedure; B, ^{1}H spectrum (using presaturation) of an extract that underwent the finalized (freeze-thaw) extraction procedure.

This technique was employed to cause further lyzing of the cells, and improved the separation between the supernatant and cellular debris. Thus, centrifuging was attempted. However, the separation that was achieved was still poor. Finally, it was decided to suspend the cells in D_2O that did not contain magnesium ions because it was observed that the magnesium ions caused coagulation. This permitted the samples to be successfully centrifuged after sonication. The addition of the freeze-thaw cycle and centrifuging techniques allowed for twice the amount of cells (four culture dishes) per sample (~16.0 x 10^6). This increase in cell concentration had a direct effect on the S/N ratio shown in the spectra of Figure 9.

3.2 Peak Identification

Phosphorous spectra for freeze-thaw extracts displayed seven distinct metabolite resonance peaks. These metabolite peaks were categorized into two groups: the low-

Reproduced with permission of the copyright owner. Further reproduction prohibited without permission.

energy phosphates (LEP) [61] that were detected in the range of 0.0 to 4.0 ppm (Figure 10), and the high-energy phosphates (HEP) [61] that were detected in the range of −10 to −14 ppm (Figure 11). An experiment studying the phosphorous metabolites of one extract over a 22 h time period was performed, and a spectrum was recorded every hour. The results from this experiment are shown in Figure 12. The identity of the inorganic peak (P_i) peak was determined because the resonance peak at 1.8 ppm increased in intensity as time passed (cellular death increased) [25, 60]. All of the other peaks decreased in intensity (Figure 12). Each of the LEP peaks was assigned by comparison with known chemical shifts of phosphorous metabolites (Table 6) [17, 31]. However, chemical shifts for HEP metabolites could not be found in literature. The literature only lists metabolites found in previously reported extraction procedures, not the method of freeze-thaw extraction that was developed in this project. Hence, different extraction procedures could yield different NMR-detectable metabolites [69-70] from those determined by perchloric acid (PCA) extracts for the MCF-7 cell line.

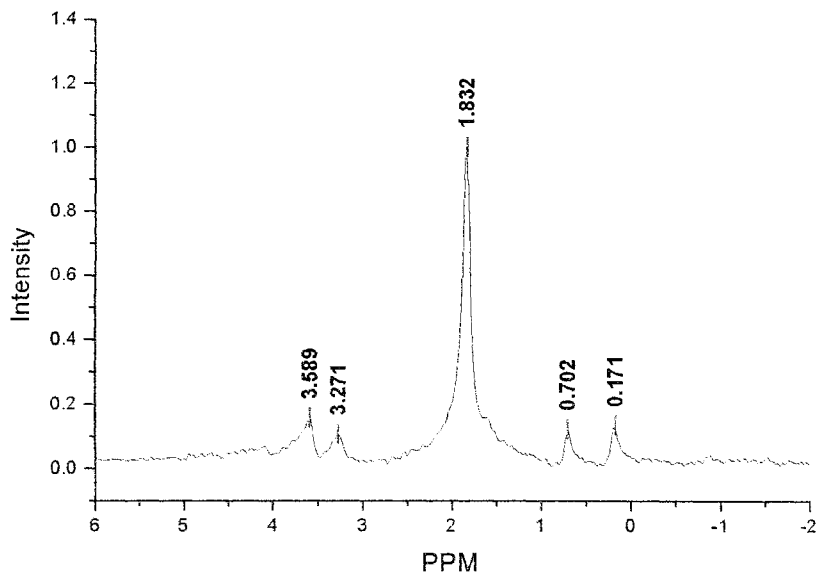

Figure 10. ^{31}P Spectrum of MCF-7 cells freeze-thaw extract displaying the LEP range.

Reproduced with permission of the copyright owner. Further reproduction prohibited without permission.

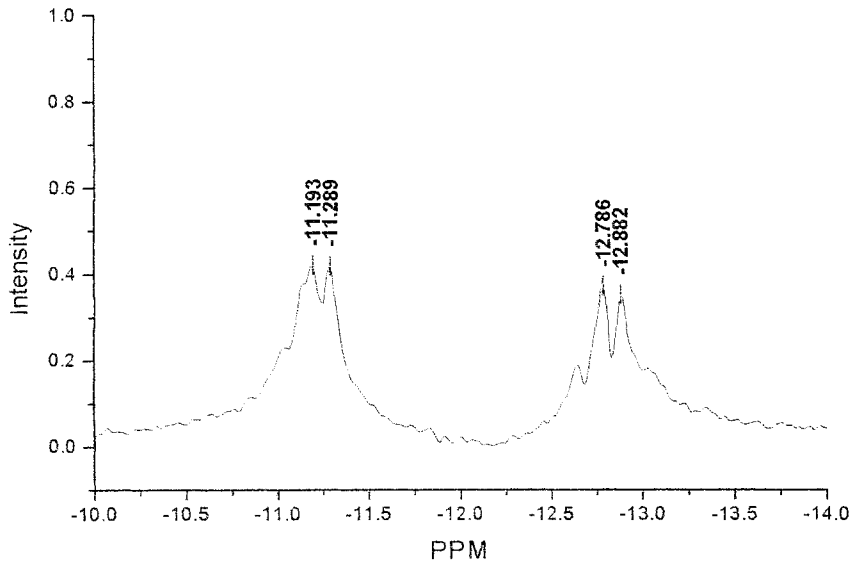

Figure 11. ^{31}P spectrum of MCF-7 cells freeze-thaw extract displaying the HEP range.

Metabolite	Literature Chemical Shift Values [19] (Respect to PCr)	Literature Chemical Shift Values [11] (Respect to GPC)	Experimental Chemical Shift Values (Respect to GPC)
PE	N/A	3.81	3.42
PC	3.12	3.51	3.10
P_i	1.82	2.51	1.66
GPE	0.44	0.6	0.53
GPC	N/A	0	0

Table 6. The ^{31}P NMR literature values [19] are referenced to phosphocreatine (PCr) at 0.00 ppm at a pH=7.2, and are fully complexed with Mg^{+2}. The ^{31}P NMR literature values [11] are referenced to glycerophosphocholine (GPC) at 0.49 ppm at a pH=7.4. ^{31}P NMR experimental values (complexed with Mg^{+2}) are referenced to GPC at 0.49 ppm at a pH=5.5, which had an effect on metabolite shifts compared to literature values [11, 19]. PE, phosphoethanolamine; PC, phosphocholine; GPE, glycerophosphoethanolamine.

Reproduced with permission of the copyright owner. Further reproduction prohibited without permission.

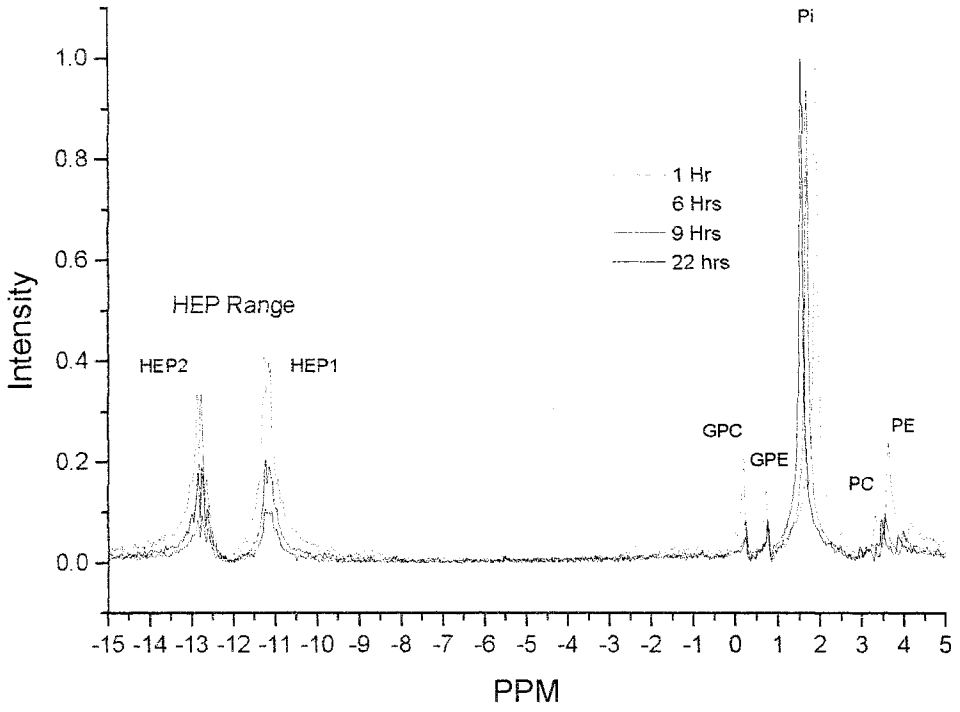

Figure 12. ^{31}P spectra of an MCF-7 control freeze-thaw extract, obtained at 1, 6, 9, and 22 h post the initial run. The P_i was normalized to 1, and peak labeling was performed using the results from Table 6.

3.3 Metabolite Stabilization

The stability of the phosphorous metabolites was a parameter that needed to be optimized to achieve the best possible reproducibility for ^{31}P spectra. Two major modifications were made in the development of the freeze-thaw extraction procedure. The first was the use of D_2O as a solvent for the extracts, and the second was the addition of the divalent ion of magnesium (Mg^{+2}) to the D_2O solvent. The effects of these improvements are shown quantitatively in Table 7 and Table 8, as percent difference values. These values report the changes in relative metabolite concentrations over time post-extraction. It can be concluded that the stability of phosphorous containing metabolites increased with the use of D_2O/Mg^{+2} as a solvent.

Reproduced with permission of the copyright owner. Further reproduction prohibited without permission.

Ratio's	Pi/PE	Pi/PC	Pi/GPE	Pi/GPC	Pi/HEP1	Pi/HEP2
2 h Post Extraction	2.9375	3.6014	4.6384	4.1000	1.6402	2.0971
Control	2.3514	2.7697	4.1712	2.6928	1.2176	1.5032
Difference	0.5860	0.8317	0.4672	1.4072	0.4226	0.5939
Percent Difference	24.92	30.03	11.20	52.26	34.70	39.51

Ratio's	Pi/PE	Pi/PC	Pi/GPE	Pi/GPC	Pi/HEP1	Pi/HEP2
4 h Post Extraction	3.3444	5.5328	6.2438	5.4239	1.9684	2.3891
Control	2.3514	2.7697	4.1712	2.6928	1.2176	1.5032
Difference	0.9929	2.7631	2.0726	2.7311	0.7508	0.8859
Percent Difference	42.23	99.76	49.69	101.42	61.66	58.94

Ratio's	Pi/PE	Pi/PC	Pi/GPE	Pi/GPC	Pi/HEP1	Pi/HEP2
6 h Post Extraction	4.0575	6.2759	6.8185	7.1464	2.2775	2.8017
Control	2.3514	2.7697	4.1712	2.6928	1.2176	1.5032
Difference	1.7060	3.5062	2.6473	4.4536	1.0599	1.2985
Percent Difference	72.55	126.59	63.47	165.39	87.05	86.38

Table 7. The control of this experiment is the initial ^{31}P NMR spectrum that was acquired immediately following extraction. This experiment was performed using BSS as a solvent. Additionally, the extraction procedure used for this experiment does not involve freeze-thawing or sonication. The resonance P_i peak was normalized to one for analysis.

Ratio's	Pi/PE	Pi/PC	Pi/GPE	Pi/GPC	Pi/HEP1	Pi/HEP2
2 h Post Extraction	6.8460	15.6764	8.9985	7.2828	2.9509	3.2757
Control	6.1862	8.2075	7.8198	6.7760	2.4515	2.7118
Difference	0.6598	7.4690	1.1786	0.5068	0.4994	0.5639
Percent Difference	10.67	91.00	15.07	7.48	20.37	20.79

Ratio's	Pi/PE	Pi/PC	Pi/GPE	Pi/GPC	Pi/HEP1	Pi/HEP2
4 h Post Extraction	7.9770	23.2558	10.0261	9.6052	3.6100	3.9826
Control	6.1862	8.2075	7.8198	6.7760	2.4515	2.7118
Difference	1.7908	15.0483	2.2062	2.8292	1.1585	1.2708
Percent Difference	28.95	183.35	28.21	41.75	47.26	46.86

Ratio's	Pi/PE	Pi/PC	Pi/GPE	Pi/GPC	Pi/HEP1	Pi/HEP2
6 h Post Extraction	9.0302	23.5239	12.4177	10.6338	4.2716	4.6635
Control	6.1862	8.2075	7.8198	6.7760	2.4515	2.7118
Difference	2.8440	15.3164	4.5979	3.8578	1.8201	1.9517
Percent Difference	45.97	186.61	58.80	56.93	74.24	71.97

Table 8. The control of this experiment is the initial ^{31}P NMR spectrum that was acquired immediately following extraction. This experiment was performed using D_2O/Mg^{+2} as a solvent. Additionally, the freeze-thaw extraction procedure was used for this experiment. The resonance P_i peak was normalized to one for analysis.

Reproduced with permission of the copyright owner. Further reproduction prohibited without permission.

The P_i peak for the corresponding ^{31}P spectra of Table 7 and Table 8 increased in intensity as time passed. However, the rest of the peaks decreased in intensity relative to the inorganic phosphate peak. The increase in P_i is a result of the breakdown of organic phosphates caused by cellular death [60]. This increase in P_i could led to the phosphorylation of other metabolites, such as choline, which could account for the large relative increase found for this metabolite in Table 7 and Table 8. It is apparent from the percent difference values reported in Table 8 that a number of reactions are still occurring during the ~40 min acquiring time of ^{31}P NMR experiments. To avoid variance in metabolite levels, it is critical to keep the time between suspension of the cellular extracts and commencement of the NMR experiment the same for all samples. Hence, the number of transients that can be performed for a ^{31}P NMR experiment is limited due to the lengthening of the acquisition time.

3.4 Reproducibility Studies

The freeze-thaw extracts were highly viscous. This resulted in line broadening of the resonance peaks for both ^{1}H and ^{31}P spectra and caused a large amount of peak overlapping in ^{1}H spectra (Figure 9.B). Subsequently, a quantitative analysis of the peak heights for metabolites in ^{1}H spectra was deemed impractical for the present analysis. An analysis was performed on ^{31}P spectral peaks. It is important to note that a single extract sample required four cell culture dishes. Due to the expense of materials such as culture dishes and growth medium as well as the large amount of space the 24 culture plates occupy in the incubator, a limit of six samples per experiment was set. For each experiment, all control samples underwent extraction simultaneously and were run one after another on the NMR the following day. All NMR experiments were conducted

Reproduced with permission of the copyright owner. Further reproduction prohibited without permission.

using identical parameters that included an acquisition temperature of 23 °C. On any given day, n spectra were obtained from separately prepared extraction samples. The peak height reproducibility of same day samples (intra-batch) is reported in Table 9 as the average standard deviation. An unknown peak (~ 4.00 ppm) was detected in a small number of spectra that were obtained for non-irradiated (control) samples. Due to the inconsistency of this unknown peak, it was not included in this quantitative study. Peak heights were measured, and the P_i resonance peak was normalized to one. There were six combinations of relative metabolite ratios determined. The standard deviation from the mean peak height values for each day is shown in Table 9. The weighted average was calculated for each peak ratio and is reported in Table 9.

$$SD_w = 1/N \, \Sigma_i \, n_i \, SD_i \qquad N = \Sigma_i \, n_i \qquad \text{(Weighted Average)}$$

- i increments the day the experiments were acquired
- SD_i = the average standard deviation values on ith day

The percent error of the weighted average values for each peak ratio is listed in Table 10. These values were used to determine the error bars for intra-batch samples.

DATE (n)	Pi/PE	Pi/PC	Pi/GPE	Pi/GPC	Pi/HEP1	Pi/HEP2
June 23 (2)	0.114	0.504	0.176	0.053	0.017	0.076
June 25 (2)	0.022	1.604	0.178	0.079	0.011	0.062
June 30 (2)	0.169	0.806	0.245	0.501	0.054	0.035
July 1 (2)	0.079	0.661	0.127	0.003	0.106	0.076
Sept 16 (3)	0.659	0.817	0.516	0.116	0.213	0.204
Sept 21 (3)	0.146	0.328	0.289	0.041	0.135	0.145
Sept 22 (3)	0.096	1.331	0.063	0.123	0.077	0.116
Sept 28 (3)	0.137	1.295	0.368	0.085	0.005	0.159
Sept 29 (3)	0.190	0.672	0.229	0.110	0.194	0.267
Oct 14 (5)	0.076	0.862	0.209	0.173	0.118	0.169
Weighted Average SD	0.173	0.885	0.246	0.127	0.101	0.143

Table 9. The standard deviation from the mean peak height ratio obtained for several independent measurements conducted on 10 different days. This value was weighted according to its value of n, in order to achieve the weighted average value for each metabolite ratio. The experiment on September 16, 2004 was the first one conducted after a two-month period where the cell line was not in use.

Reproduced with permission of the copyright owner. Further reproduction prohibited without permission.

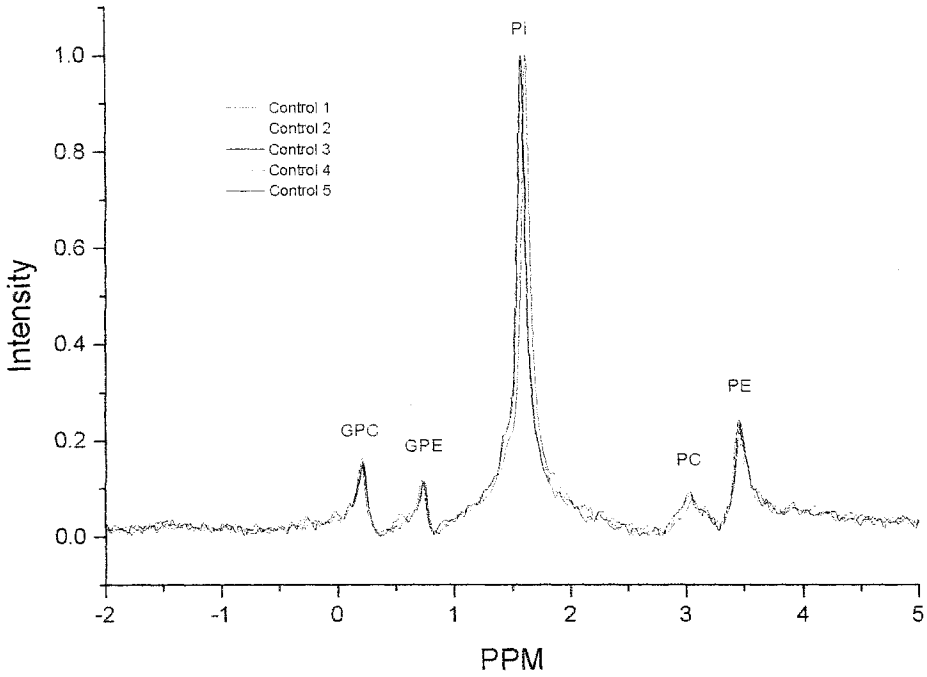

Figure 13. ^{31}P spectra of the LEP range of five control samples obtained on October 14, 2004.

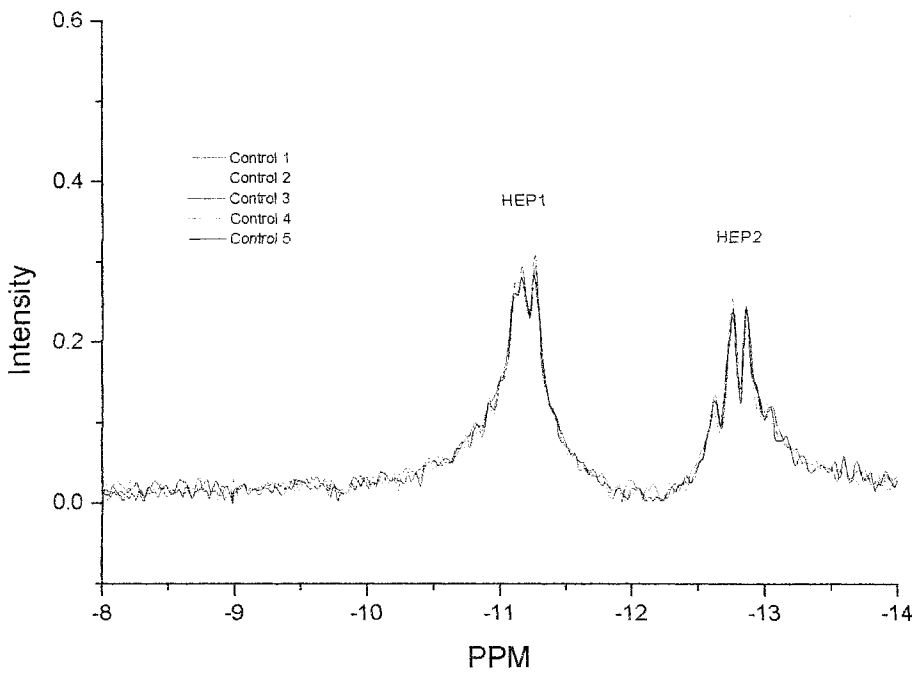

Figure 14. ^{31}P spectra of the HEP range of five control samples obtained on October 14, 2004.

Reproduced with permission of the copyright owner. Further reproduction prohibited without permission.

DATE (n)	Pi/PE	Pi/PC	Pi/GPE	Pi/GPC	Pi/HEP1	Pi/HEP2
June 23 (2)	2.772	4.986	2.549	1.104	0.697	2.630
June 25 (2)	0.778	15.065	2.962	2.009	0.310	1.335
June 30 (2)	2.688	9.178	3.068	7.031	2.241	1.273
July 1 (2)	1.298	6.256	2.354	0.097	3.052	2.016
Sept 16 (3)	8.721	7.214	6.340	2.661	4.742	3.703
Sept 21 (3)	4.860	5.133	6.425	1.799	4.581	4.137
Sept 22 (3)	2.492	10.976	0.953	3.074	2.239	2.709
Sept 28 (3)	2.083	9.152	5.016	1.774	0.126	3.320
Sept 29 (3)	2.387	6.172	3.488	2.881	4.289	4.844
Oct 14 (5)	1.800	7.275	2.412	2.744	3.457	4.067
Weighted SD Error	3.061	7.975	3.593	2.528	2.779	3.249

Table 10. The percent standard deviation from the mean peak height ratio is given. This value was weighted according to its value of n, in order to achieve the weighted average error value for each metabolite ratio. The percent error reports the deviations in reproducibility for intra-batch control samples.

As an example, the five ^{31}P spectra that were acquired on October 14, 2004 are shown in Figure 13 and Figure 14. The corresponding statistics are listed in Tables 9 and 10. The average peak height ratio, average standard deviation and percent error for control samples that were acquired on different days are shown in Table 11. The values reported in Table 11 show quantitatively that inter-batch control samples have largely inconsistent reproducibility when compared to the intra-batch control samples (Tables 9 and 10). The lack of reproducibility is illustrated in Figures 15 and 16. These figures compare ^{31}P spectra that were acquired on three different experimental days using identical NMR parameters and extraction procedures. The percent error of the average values for each peak ratio, listed in Table 11, determined the error bars for inter-batch control samples. The results of both reproducibility studies (Tables 10 and 11) cannot be effectively compared to the values found in the literature because there are no previously reported reproducibility studies. Literature provides some graphical (error bars) and tabulated standard deviation values [28, 49, 61].

Reproduced with permission of the copyright owner. Further reproduction prohibited without permission.

DATE	Pi/PE	Pi/PC	Pi/GPE	Pi/GPC	Pi/HEP1	Pi/HEP2
June 23	4.106	10.116	6.896	4.773	2.439	2.885
June 25	2.786	10.647	5.995	3.936	3.495	4.632
June 30	6.306	8.777	7.993	7.131	2.413	2.736
July 1	6.077	10.566	5.415	3.502	3.458	3.792
Sept 16	7.552	11.318	8.145	4.341	4.487	5.513
Sept 21	3.013	6.381	4.492	2.258	2.944	3.504
Sept 22	3.868	12.128	6.572	4.009	3.446	4.269
Sept 28	6.582	14.151	7.346	4.795	4.047	4.794
Sept 29	7.970	10.887	6.558	3.810	4.519	5.521
Oct 14	4.215	11.842	8.649	6.306	3.422	4.149
Average	4.771	9.710	6.187	4.078	3.152	3.800
Average SD	2.381	3.770	2.389	1.890	1.259	1.563
Percent Error	49.899	38.820	38.612	46.344	39.952	41.122

Table 11. The average peak height ratio, average standard deviation, and percent error are given. The average SD is calculated from the mean peak height ratio. The percent error reports the deviations in reproducibility for inter-batch control samples.

However, these values are for specific doses of irradiation and chemotherapy treatments that do not directly relate to the non-irradiated control samples in this study. Therefore, no reasonable quantitative comparisons can be drawn.

The increase in standard deviation and percent error values for inter-batch samples compared to intra-batch samples could be attributed to varying spin-lattice (T_1) relaxation times. This inconsistency of T_1 values would affect each particular metabolite signal in varying degrees, causing an overall change in the relative intensities of metabolite peak ratios found in NMR spectra. Inconsistencies for inter-batch samples could also be due to growth fraction variance. The term growth fraction refers to the proportion of proliferating cells in the cell cycle [4]. The cell cycle is composed of four different phases: S (DNA synthesis), M (mitosis), and the gaps that precede and follow the S phase, G1 and G2 respectively [4]. It has been reported in literature [80] that variations of growth fractions can be found throughout cell culturing passages.

Reproduced with permission of the copyright owner. Further reproduction prohibited without permission.

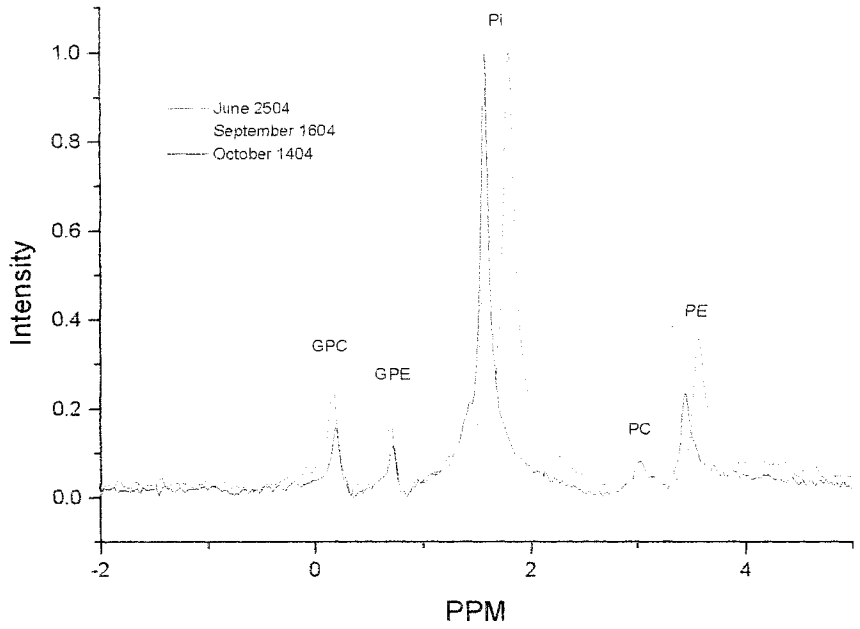

Figure 15. ^{31}P spectra of the LEP range for three control samples run on June 25, 2004, September 16, 2004, and October 14, 2004.

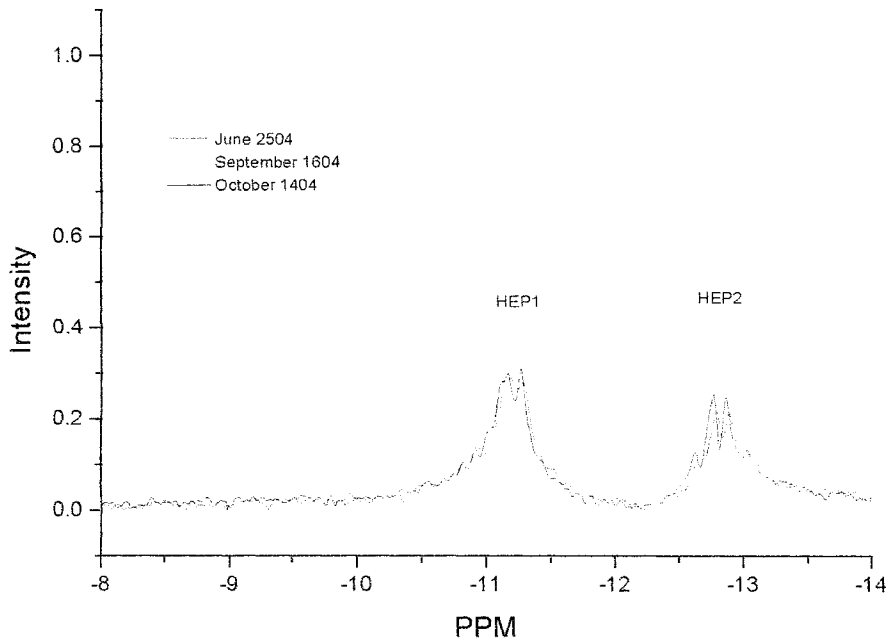

Figure 16. ^{31}P spectra of the HEP range for three control samples run on June 25, 2004, September 16, 2004, and October 14, 2004.

Reproduced with permission of the copyright owner. Further reproduction prohibited without permission.

Therefore, differences in the relative amounts of metabolites found in inter-batch samples could be a major contributor to the variation in the reproducibility [52]. From the results found in this reproducibility study, it can be concluded that at least one non-irradiated (control) sample will be required for each irradiation run. This ensures that spectral reproducibility corresponds to the intra-batch standard deviation values for each experiment. Without a control sample, only relative radiation dose quantifications would be possible for each experiment.

3.5 Preliminary Irradiation Studies

The reproducibility study indicated that in order to minimize the standard deviations in irradiation experiments a control sample would be required for every experiment. The initial step for this preliminary study was to determine the delay time between irradiation and freeze-thaw extraction that displays the maximum degree of change in the relative metabolite intensities. For all irradiation experiments, the amount of radiation delivered was within the possible therapeutic doses used for radiation therapy. Therefore, the results yielded useful information about therapeutic treatment effects. It has been reported [59] that there are two distinct stages of cellular repair that occur post-irradiation. Each stage can result in different relative metabolite intensity levels. The first stage is the transient stage. This occurs immediately following irradiation and lasts up to approximately 3 h post-irradiation [59]. The second is the steady-state stage of repair, which reportedly lasts up to seven days post-irradiation [49, 61]. For this preliminary study, three different times post-irradiation were examined. These times covered both stages of repair. To explore the transient stage of repair, a spectrum was acquired at a time of two hours post-irradiation (Figure 17).

Reproduced with permission of the copyright owner. Further reproduction prohibited without permission.

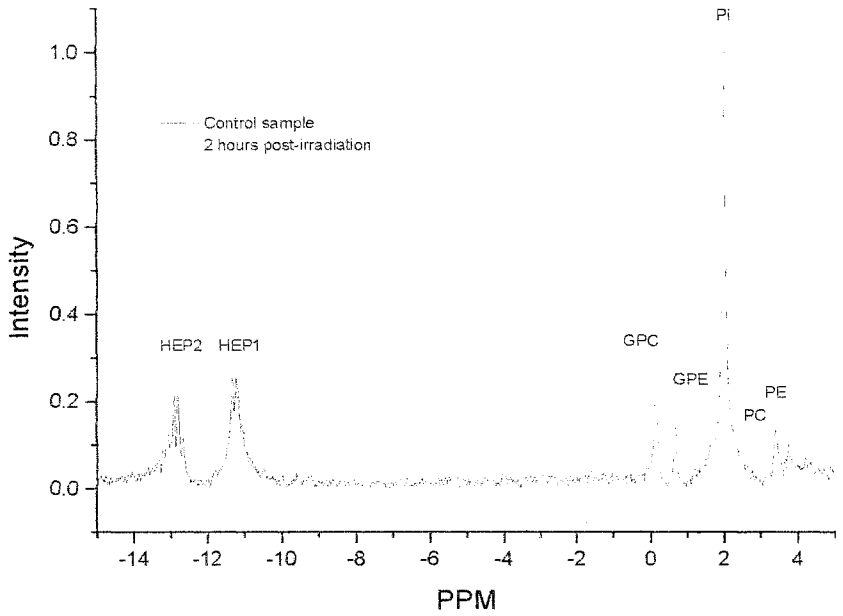

Figure 17. ^{31}P spectra of MCF-7 cell extracts. A non-irradiated 'control' sample (red) is compared to a sample that received 8 Gy and was acquired two hours post-irradiation (green).

Ratio's	Pi/PE	Pi/PC	Pi/GPE	Pi/GPC	Pi/HEP1	Pi/HEP2
8 Gy	7.009	9.967	7.390	3.769	4.531	5.590
Control	9.793	17.606	7.144	3.736	3.877	4.595
Difference	-2.7842	-7.8392	0.2460	0.0322	0.6542	0.9958
Percent Difference	28.43	44.02	3.44	0.86	16.87	21.67

Table 12. ^{31}P spectra were acquired for an irradiation sample two hours following irradiation and a control sample. The resonance P_i peak was normalized to one for analysis. These values are indicators of the degree of change that occurred in the relative metabolite levels due to radiation (8 Gy).

The irradiation sample in this experiment was given a dose of 8 Gy. The quantitative changes that occurred between the irradiated spectrum and the control spectrum are shown in Table 12. The P_i/HEP1 and P_i/HEP2 ratio values increased for the irradiation sample compared to the control. The largest change in ratio values occurred for the P_i/PE and P_i/PC ratios. To examine the steady-state stage of repair, the cells were examined 24 and 48 hours post-irradiation were examined.

Reproduced with permission of the copyright owner. Further reproduction prohibited without permission.

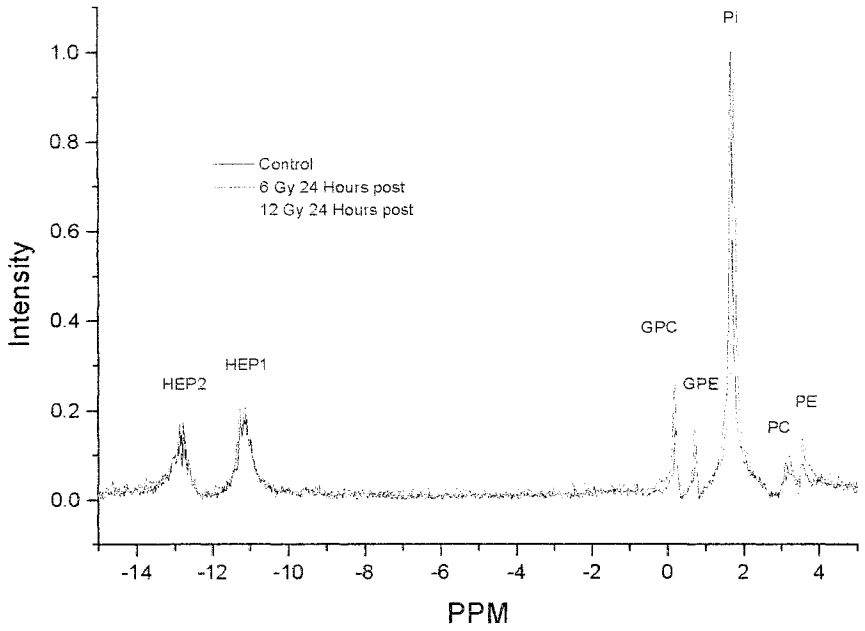

Figure 18. ^{31}P spectra of MCF-7 cell extracts. A non-irradiated 'control' sample (blue) is compared to a sample that received 6 Gy (red) and a sample that received 12 Gy (green). Both irradiated samples were acquired 24 hours post-irradiation.

For this experiment, the doses of 6 Gy and 12 Gy were used for both 24 and 48 hours post-irradiation. The spectral changes for both doses at 24 hours post-irradiation are shown in Figure 18, and for 48 hours, the spectra are shown in Figure 19. The quantitative changes for 24 and 48 hours post-irradiation at the dose of 6 Gy are reported in Table 13. The corresponding data for 12 Gy is reported in Table 14. It should be noted that the experimental procedure used for the steady state experiment had a variation compared to the procedure used in the transient experiment. The difference was that the control sample was re-plated on the day of irradiation because the density of the cells was higher than optimal. This effect could also impact the irradiation samples. This higher than normal cell density could cause a decrease in cell proliferation and alter the growth fraction for this experiment.

Reproduced with permission of the copyright owner. Further reproduction prohibited without permission.

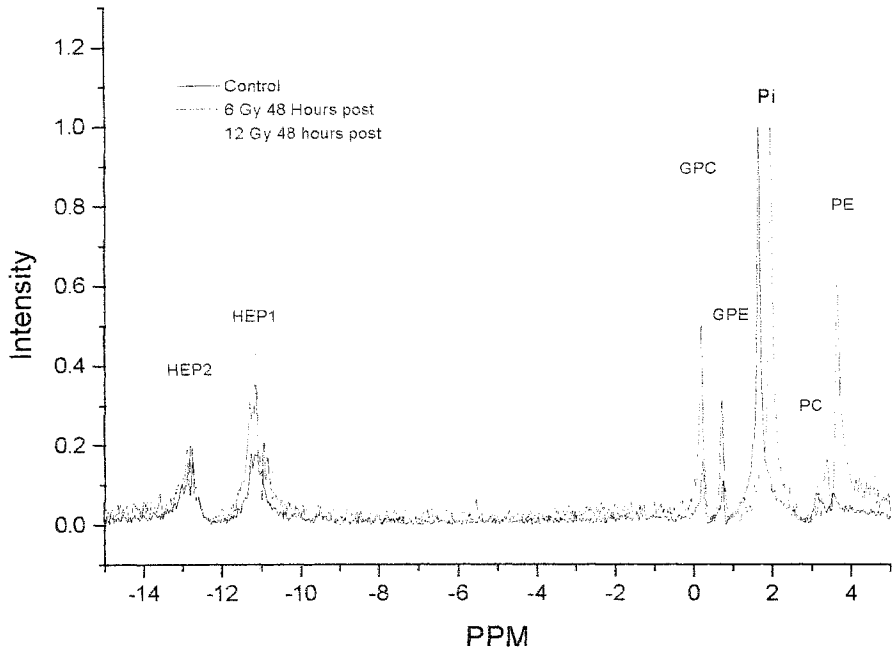

Figure 19. ^{31}P spectra of MCF-7 cell extracts. A control sample (blue) is compared to a sample that received 6 Gy (red) and a sample that received 12 Gy (green). Both irradiated samples were acquired 48 hours post-irradiation.

Therefore, the degree of change present in post-irradiation spectra may have been altered due to a variation in the growth fraction of the samples [81]. The P_i/HEP1 and P_i/HEP2 ratio values decreased for all of the irradiation samples compared to the control, except for the 6 Gy dose at 24 hours post-irradiation. All of the metabolite ratios, except for P_i/HEP1 and P_i/HEP2 ratios, showed a decrease in ratio values for irradiated samples compared to the control sample. The largest change in ratio values occurred at 48 hours post-irradiation. This change was in the phospholipid range, which consisted of GPE, GPC, PE, and PC metabolites. These findings correspond to previously reported [57-62] studies, which concluded that the phospholipid metabolite range was the most sensitive to radiation treatment. This preliminary study, which encompassed only a small number of times post-irradiation, indicated that 48 hrs post-irradiation yielded the most significant changes.

Reproduced with permission of the copyright owner. Further reproduction prohibited without permission.

Ratio's	Pi/PE	Pi/PC	Pi/GPE	Pi/GPC	Pi/HEP1	Pi/HEP2
6Gy (24hrs post)	7.241	1.002	6.329	3.832	4.833	5.793
Control	10.985	9.991	8.841	6.367	4.776	5.631
Difference	-3.7442	-8.9894	-2.5118	-2.5356	0.0574	0.1620
Percent Difference	34.09	89.97	28.41	39.82	1.20	2.88

Ratio's	Pi/PE	Pi/PC	Pi/GPE	Pi/GPC	Pi/HEP1	Pi/HEP2
6Gy (48hrs post)	1.629	7.805	3.206	1.987	2.982	5.048
Control	10.985	9.991	8.841	6.367	4.776	5.631
Difference	-9.3559	-2.1858	-5.6346	-4.3801	-1.7940	-0.5824
Percent Difference	85.17	21.88	63.74	68.79	37.57	10.34

Table 13. ^{31}P spectra were acquired for the irradiation samples at 24 and 48 hours post-irradiation. The resonance P_i peak was normalized to one for analysis. These values are indicators of the degree of change that occurred in the relative metabolite levels due to radiation (6 Gy).

Ratio's	Pi/PE	Pi/PC	Pi/GPE	Pi/GPC	Pi/HEP1	Pi/HEP1
12Gy (24hrs post)	8.706	8.452	5.335	3.139	4.515	5.797
Control	10.985	9.991	8.841	6.367	4.776	5.631
Difference	-2.2785	-1.5394	-3.5058	-3.2282	-0.2606	0.1659
Percent Difference	20.74	15.41	39.66	50.70	5.46	2.95

Ratio's	Pi/PE	Pi/PC	Pi/GPE	Pi/GPC	Pi/HEP1	Pi/HEP2
12Gy (48hrs post)	1.335	3.691	2.224	1.203	2.353	3.247
Control	10.985	9.991	8.841	6.367	4.776	5.631
Difference	-9.6496	-6.2996	-6.6163	-5.1641	-2.4224	-2.3839
Percent Difference	87.85	63.05	74.84	81.10	50.72	42.34

Table 14. ^{31}P spectra were acquired for the irradiation samples at 24 and 48 hours post-irradiation. The resonance P_i peak was normalized to one for analysis. These values are indicators of the degree of change that occurred in the relative metabolite levels due to radiation (12 Gy).

Subsequently, a time delay of 48 hours was chosen for a response versus dose relationship study. Two different ranges of doses were used for this study. The first consisted of 4, 6, 8 and 12 Gy. The second study used a dose range of 4.5, 5, 5.5, 6, and 8.5 Gy. Both experiments followed the same experimental procedures. The resultant ^{31}P spectra for both irradiation experiments are shown in Figures 20-24. These spectra are expanded in the two ranges of interest.

Reproduced with permission of the copyright owner. Further reproduction prohibited without permission.

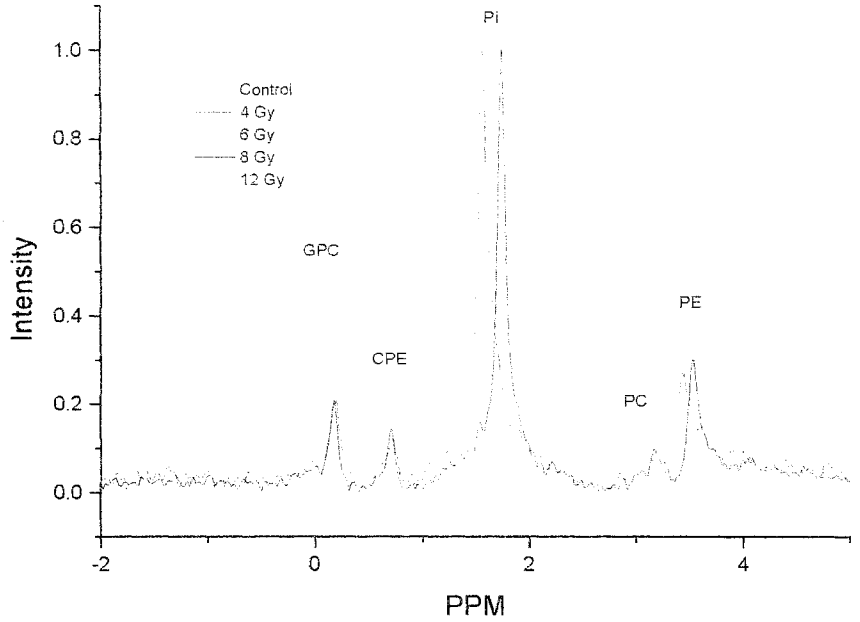

Figure 20. ^{31}P spectra of the LEP range for MCF-7 cell extracts. A control sample (dark yellow) is compared to samples that received 4 Gy (red), 6 Gy (green), 8 Gy (blue), and 12 Gy (Cyan). All of the irradiated samples were acquired at 48 hours post-irradiation.

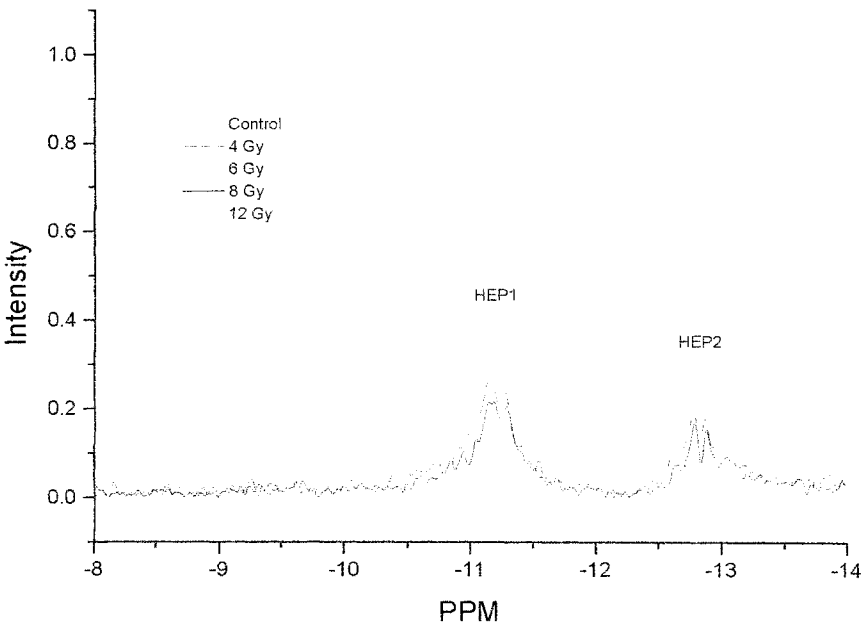

Figure 21. ^{31}P spectra of the HEP range for MCF-7 cell extracts. A control sample (dark yellow) is compared to samples that received 4 Gy (red), 6 Gy (green), 8 Gy (blue), and 12 Gy (Cyan). All of the irradiated samples were acquired at 48 hours post-irradiation.

Reproduced with permission of the copyright owner. Further reproduction prohibited without permission.

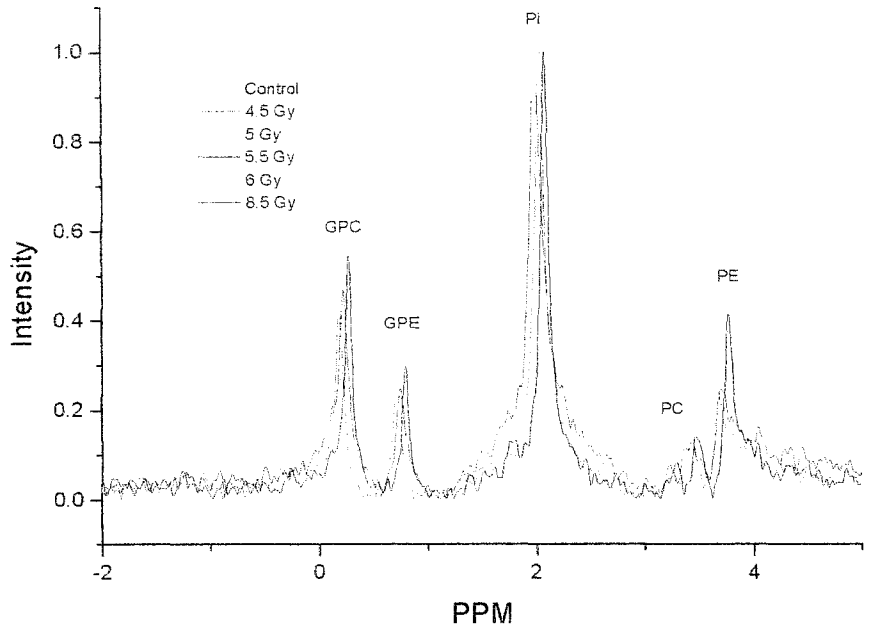

Figure 22. ^{31}P spectra of the LEP range for MCF-7 cell extracts. A control sample (dark yellow) is compared to samples that received 4.5 Gy (red), 5 Gy (green), 5.5 Gy (blue), 6 Gy (Cyan), and 8.5 Gy (black). All of the irradiated samples were acquired at 48 hours post-irradiation.

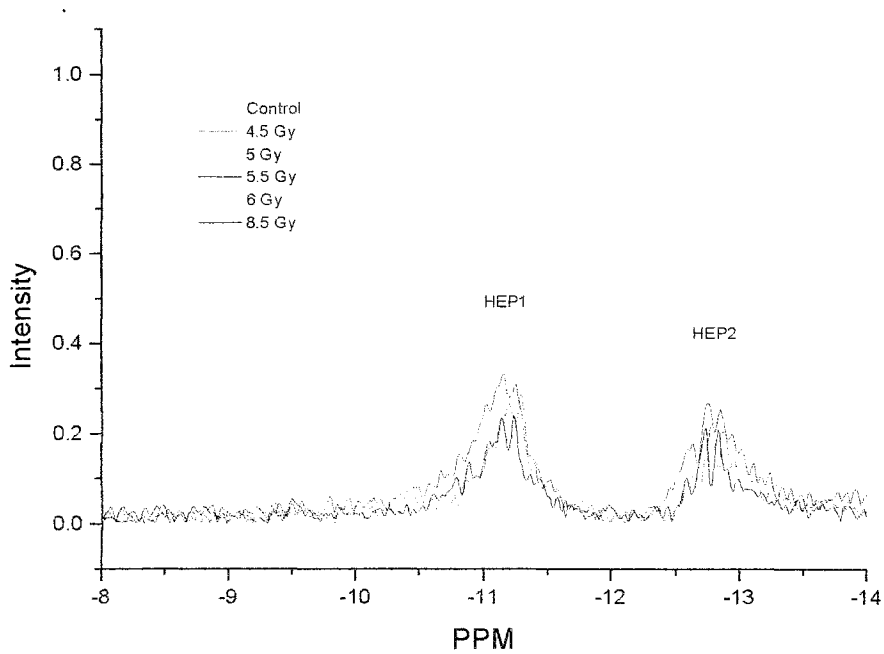

Figure 23. ^{31}P spectra of the HEP range for MCF-7 cell extracts. A control sample (dark yellow) is compared to samples that received 4.5 Gy (red), 5 Gy (green), 5.5 Gy (blue), 6 Gy (Cyan), and 8.5 Gy (black). All of the irradiated samples were acquired at 48 hours post-irradiation.

Reproduced with permission of the copyright owner. Further reproduction prohibited without permission.

The quantative changes in peak height ratios for the first dose range, which corresponds to Figures 20 and 21, are reported in Table 15. The relative quantative changes for the second study, which corresponds to Figures 22 and 23, are reported in Table 16. In the results of the first irradiation study, shown in Table 15, the value of P_i/PE and P_i/GPE ratios decreased as the dose increased. However, in both irradiation studies, only these two metabolite ratios displayed any discernable pattern related to dose. The dose-dependent changes for each particular metabolite ratio were graphically examined. The control metabolite ratio was included for each experiment as the point of zero dose. A linear fit was performed on each set of metabolite ratios (Figures 24- 29).

Ratio's	Pi/PE	Pi/PC	Pi/GPE	Pi/GPC	Pi/HEP1	Pi/HEP2
4Gy (48 hrs post)	3.704	12.194	8.105	4.719	3.964	5.438
Control	4.052	9.500	9.264	8.012	3.322	4.193
Difference	-0.3483	2.6933	-1.1585	-3.2927	0.6421	1.2448
Percent Difference	8.60	28.35	12.51	41.10	19.33	29.69

Ratio's	Pi/PE	Pi/PC	Pi/GPE	Pi/GPC	Pi/HEP1	Pi/HEP2
6Gy (48 hrs post)	3.581	9.218	7.077	4.952	4.553	5.209
Control	4.052	9.500	9.264	8.012	3.322	4.193
Difference	-0.4714	-0.2820	-2.1864	-3.0602	1.2310	1.0160
Percent Difference	11.63	2.97	23.60	38.19	37.05	24.23

Ratio's	Pi/PE	Pi/PC	Pi/GPE	Pi/GPC	Pi/HEP1	Pi/HEP2
8Gy (48 hrs post)	3.330	10.245	6.933	4.782	4.725	6.188
Control	4.052	9.500	9.264	8.012	3.322	4.193
Difference	-0.7219	0.7446	-2.3307	-3.2298	1.4031	1.9948
Percent Difference	17.82	7.84	25.16	40.31	42.23	47.58

Ratio's	Pi/PE	Pi/PC	Pi/GPE	Pi/GPC	Pi/HEP1	Pi/HEP2
12Gy (48 hrs post)	2.798	6.160	4.807	2.108	4.220	5.452
Control	4.052	9.500	9.264	8.012	3.322	4.193
Difference	-1.2536	-3.3408	-4.4565	-5.9044	0.8980	1.2589
Percent Difference	30.94	35.16	48.11	73.69	27.03	30.03

Table 15. ^{31}P spectra were acquired for the irradiation samples at 48 hours post-irradiation. These values are indicators of the degree of change that occurred in the relative metabolite levels due to the various radiation doses of 4, 6, 8, and 12 Gy.

Reproduced with permission of the copyright owner. Further reproduction prohibited without permission.

Ratio's	Pi/PE	Pi/PC	Pi/GPE	Pi/GPC	Pi/HEP1	Pi/HEP2
4.5Gy (48 hrs post)	3.917	7.920	4.437	2.423	3.707	4.667
Control	7.158	8.499	5.982	3.510	3.650	4.084
Difference	-3.2404	-0.5795	-1.5454	-1.0869	0.0576	0.5824
Percent Difference	45.27	6.82	25.83	30.97	1.58	14.26

Ratio's	Pi/PE	Pi/PC	Pi/GPE	Pi/GPC	Pi/HEP1	Pi/HEP2
5Gy (48 hrs post)	3.690	8.232	3.460	1.829	4.055	4.962
Control	7.158	8.499	5.982	3.510	3.650	4.084
Difference	-3.4681	-0.2673	-2.5215	-1.6813	0.4050	0.8780
Percent Difference	48.45	3.14	42.15	47.90	11.10	21.50

Ratio's	Pi/PE	Pi/PC	Pi/GPE	Pi/GPC	Pi/HEP1	Pi/HEP2
5.5Gy (48 hrs post)	4.069	7.336	4.033	2.129	3.119	3.840
Control	7.158	8.499	5.982	3.510	3.650	4.084
Difference	-3.0883	-1.1634	-1.9487	-1.3808	-0.5309	-0.2443
Percent Difference	43.15	13.69	32.58	39.34	14.55	5.98

Ratio's	Pi/PE	Pi/PC	Pi/GPE	Pi/GPC	Pi/HEP1	Pi/HEP2
6Gy (48 hrs post)	3.917	7.695	4.468	2.302	3.533	4.484
Control	7.158	8.499	5.982	3.510	3.650	4.084
Difference	-3.2404	-0.8038	-1.5135	-1.2084	-0.1166	0.4002
Percent Difference	45.27	9.46	25.30	34.43	3.20	9.80

Ratio's	Pi/PE	Pi/PC	Pi/GPE	Pi/GPC	Pi/HEP1	Pi/HEP2
8.5Gy (48hrs post)	2.407	7.063	3.357	1.827	4.261	4.750
Control	7.158	8.499	5.982	3.510	3.650	4.084
Difference	-4.7511	-1.4359	-2.6253	-1.6832	0.6117	0.6658
Percent Difference	66.38	16.90	43.89	47.95	16.76	16.30

Table 16. ^{31}P spectra were acquired for the irradiation samples at 48 hours post-irradiation. These values are indicators of the degree of change that occurred in the relative metabolite levels due to the various radiation doses of 4.5, 5, 5.5, 6, and 8.5 Gy.

The metabolite ratios of P_i/PE (Figure 24), and P_i/GPC (Figure 27) showed a similar trend in behaviour for both irradiation experiments when plotted as a function of dose. With a limited number of points provided by these preliminary studies, there are a large number of graphical fits that could be made. However, characteristic patterns in the overall change in metabolite ratios are still present. There appears to be a scaling issue in the slope and y-intercept between runs from different days. This scaling issue is likely caused by a similar effect that leads to poor reproducibility in inter-batch control experiments.

Reproduced with permission of the copyright owner. Further reproduction prohibited without permission.

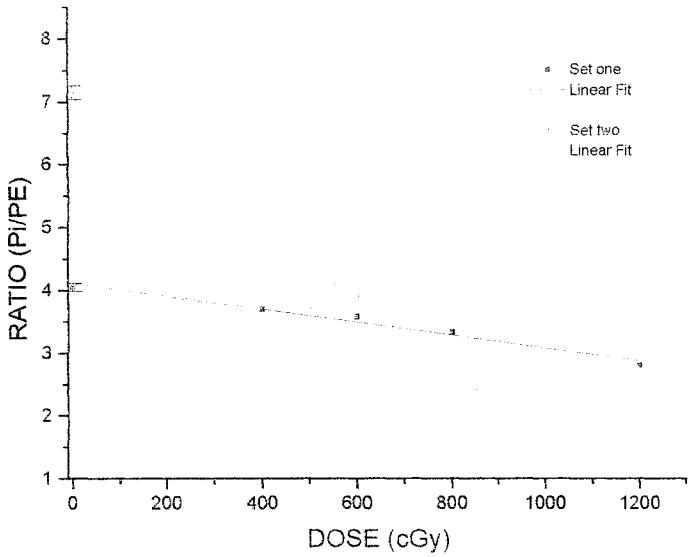

Figure 24. A linear fit of the metabolite ratio P_i/PE values for set one that consists of 4, 6, 8, and 12 Gy doses, and set two consist of 4.5, 5, 5.5, 6, and 8.5 Gy doses. An Error bar of 1.47 percent was placed on the control metabolite ratio, which was obtained from Table 10. The correlation coefficients for set one are 4.113 and –0.001 with a p-value of 0.001. The correlation coefficients for set two are 6.952 and –0.006 with a p-value of 6.35×10^{-4}.

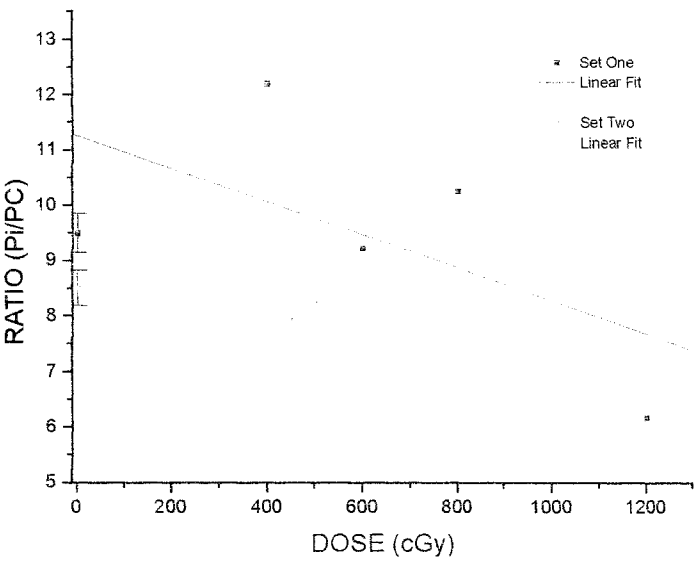

Figure 25. A linear fit of the metabolite ratio P_i/PC values for set one that consists of 4, 6, 8, and 12 Gy doses, and set two consist of 4.5, 5, 5.5, 6, and 8.5 Gy doses. An Error bar of 3.74 percent was placed on the control metabolite ratio, which was obtained from Table 10. The correlation coefficients for set one are 11.259 and –0.003 with a p-value of 0.271. The correlation coefficients for set two are 8.613 and –0.002 with a p-value of 0.027.

Reproduced with permission of the copyright owner. Further reproduction prohibited without permission.

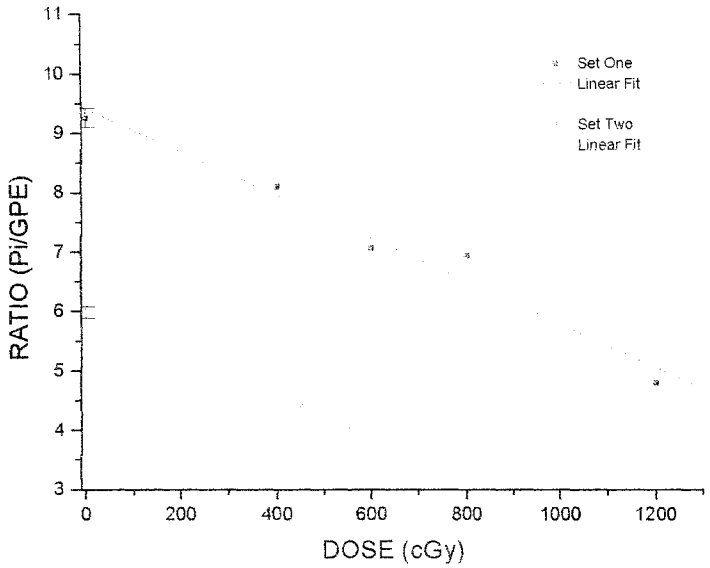

Figure 26. A linear fit of the metabolite ratio P_i/GPE values for set one that consists of 4, 6, 8, and 12 Gy doses, and set two consist of 4.5, 5, 5.5, 6, and 8.5 Gy doses. An Error bar of 1.71 percent was placed on the control metabolite ratio, which was obtained from Table 10. The correlation coefficients for set one are 9.418 and –0.004 with a p-value of 0.002. The correlation coefficients for set two are 5.470 and –0.002 with a p-value of 0.140.

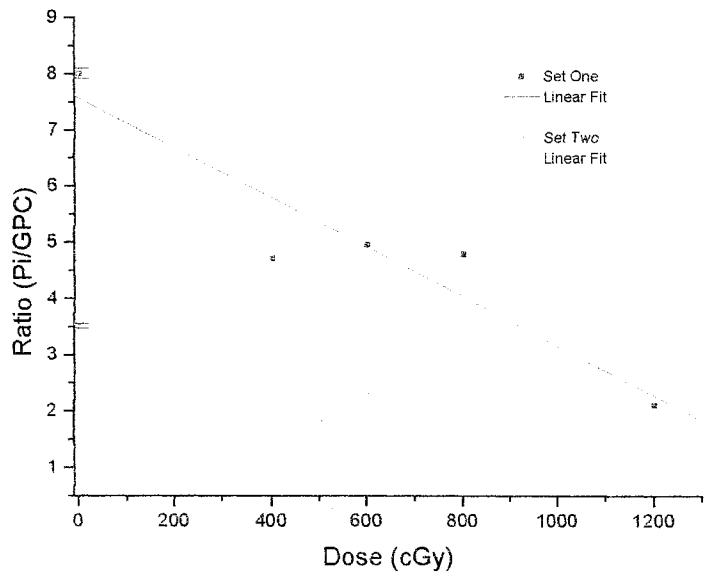

Figure 27. A linear fit of the metabolite ratio P_i/GPC values for set one that consists of 4, 6, 8, and 12 Gy doses, and set two consist of 4.5, 5, 5.5, 6, and 8.5 Gy doses. An Error bar of 1.2 percent was placed on the control metabolite ratio, which was obtained from Table 10. The correlation coefficients for set one are 7.562 and –0.004 with a p-value of 0.016. The correlation coefficients for set two are 3.332 and –0.002 with a p-value of 0.014.

Reproduced with permission of the copyright owner. Further reproduction prohibited without permission.

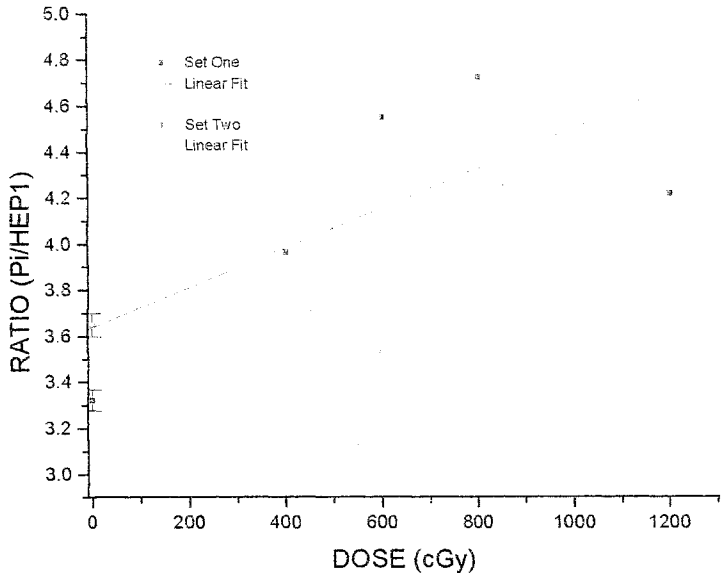

Figure 28. A linear fit of the metabolite ratio P_i/HEP1 values for set one that consists of 4, 6, 8, and 12 Gy doses, and set two consist of 4.5, 5, 5.5, 6, and 8.5 Gy doses. An Error bar of 1.37 percent was placed on the control metabolite ratio, which was obtained from Table 10. The correlation coefficients for set one are 3.64 and 8.64×10^{-4} with a p-value of 0.188. The correlation coefficients for set two are 3.50 and 4.56 with a p-value of 0.542.

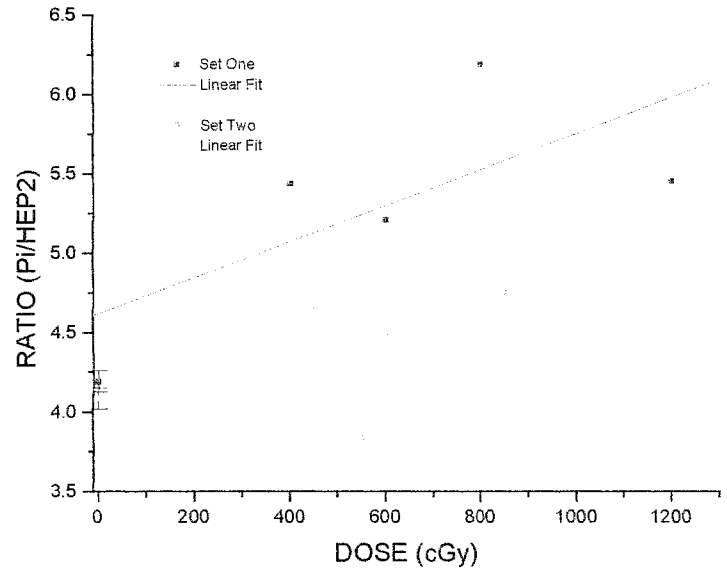

Figure 29. A linear fit of the metabolite ratio P_i/HEP2 values for set one that consists of 4, 6, 8, and 12 Gy doses, and set two consist of 4.5, 5, 5.5, 6, and 8.5 Gy doses. An Error bar of 1.6 percent was placed on the control metabolite ratio, which was obtained from Table 10. The correlation coefficients for set one are 4.617 and 0.001 with a p-value of 0.184. The correlation coefficients for set two are 4.146 and 6.477×10^{-4} with a p-value of 0.403.

Reproduced with permission of the copyright owner. Further reproduction prohibited without permission.

It was also found that a direct correlation exists between the amount of irradiation delivered and the changes in metabolite intensities for the MCF-7 cell line. It can be seen quantitatively and qualitatively that a dose difference of 50 cGy can be detected in the relative metabolite ratios of MCF-7 cell line extracts. The exact graphical determination of the effects of irradiation on specific metabolite ratios will need to be explored through a variety of different dose experiments. These experiments will help define the dose-relationship and its spectral reproducibility for each particular metabolite found using this extraction procedure. Based on these preliminary results, it has been shown that ^{31}P NMR can be used to monitor the effects of radiation therapy and, potentially, can be used to model the changes that occur in metabolites post-irradiation.

4.0 Conclusion

The most notable achievement of this research project was the development of a new procedure for cellular metabolite extraction. A number of modifications were performed throughout the development of the freeze-thaw extraction procedure. These changes optimized parameters such as cell handling techniques, temporal stability, and signal-to-noise ratio values. All of these individual parameters, combined, optimized the overall reproducibility of ^{31}P and ^{1}H spectra. This new method of extraction could lead to new insights into the changes that occur in cellular metabolite levels following treatment.

Additionally, an extensive reproducibility study was performed on the control samples. This particular type of study has not been previously reported. The results from this study indicate that the reproducibility of intra-batch samples was much higher than that of inter-batch samples. The percent error values for intra-batch samples ranged from

Reproduced with permission of the copyright owner. Further reproduction prohibited without permission.

2.53 % to 7.98 % for all the different relative metabolite ratios, and for inter-batch samples, the values ranged from 38.61 % to 49.90 %.

Finally, the preliminary irradiation study in this project examined the effected delay time between irradiation and freeze-thaw extraction. The post-irradiation times of 2, 24 and 48 h were chosen. The time of 48 h post-irradiation was determined to have the greatest quantitative change in ^{31}P spectra, and therefore, it was concluded to yield the highest sensitivity. As a result of these findings, a range of doses (4 to 12 Gy) was examined at 48 h post-irradiation. A qualitative examination of peak height ratios was performed for all of the phosphorous metabolites found in MCF-7 extracts. It was determined that a direct correlation exists between the amount of irradiation delivered, and the changes in metabolite intensities for the MCF-7 cell line. Therefore, based on these preliminary results, it has been shown that ^{31}P NMR can be used to monitor the effects of radiation therapy and, potentially, to quantify a dose-response relationship.

4.0 Future Work

There are a number of modifications that could improve the reproducibility of ^{31}P spectra for intra-batch and inter-batch samples. The simplest modification would be to monitor the confluency of the cell culture dishes in order to ensure the same cell population for all samples. Another modification would be the implementation of cell synchronization. This process fixes the cells in a particular phase (M, G_1, G_2 or S) depending on the reagent chosen. Therefore, with a large percentage of the cells (~ 80-90%) in one particular phase, the metabolite levels for all samples would be essentially fixed. Hence, samples run on the same day could potentially show improved

Reproduced with permission of the copyright owner. Further reproduction prohibited without permission.

reproducibility. More importantly, this process could have a greater effect on the reproducibility of samples from different days.

Spectral reproducibility could be improved with a spin-lattice (T_1) relaxation time study. This study would examine variations in the T_1 values for the metabolites detected in ^{31}P spectra of intra-batch and inter-batch samples. If T_1 values show differences, this would have a direct effect on the relative intensity of each metabolite. Therefore, a modification that would resolve this problem could be implemented. This could be something as simple as a longer inter-pulse delay period (> 3 x longest T1) or the addition of a relaxation agent (fixed concentration), guaranteeing full relaxation of all the metabolite signals.

The last modification that could be made to improve reproducibility would be to use a different quantitative analysis method. The method of integration (peak area) would determine the relative total metabolite concentration. This new statistical analysis could correlate the changes found in each metabolite ratio. This would result in a characterization of the system as a whole. Also, the use of a Gaussian or Lorentzian curve fitting should be investigated.

Both integration and curve fitting will require an improvement in S/N. The use of filtration would reduce the cellular debris in samples and therefore, enhance the signal-to-noise ratio. The decrease in cellular debris would also allow for a higher concentration of cells per sample that would yield a higher S/N ratio. The reduction in cellular debris would also create more mobility for the cellular metabolites, which would reduce the broadening of the peaks in both ^{31}P and ^{1}H spectra. The reduction in broadening effects

Reproduced with permission of the copyright owner. Further reproduction prohibited without permission.

would largely improve ^{1}H spectra and therefore, the same method of quantification used for the metabolites in ^{31}P spectra would be used for ^{1}H spectra.

It is apparent, from the preliminary results in this project, that the standard deviations of control samples may not be applicable for irradiation sample reproducibility. To provide standard deviations of irradiated samples, reproducibility studies, similar to those previously performed for control samples, will be required. On the other hand, two control samples could be used for each irradiation experiment. In this experiment, one control would receive the maximum dose, and the other control would receive the minimum dose for the range used. The reproducibility of irradiated runs would have to be tested because the determined control reproducibility may not apply to the reproducibility of irradiated samples at a specific dose.

Reproduced with permission of the copyright owner. Further reproduction prohibited without permission.

6.0 REFERENCES

1. Novartis Pharmaceuticals Corporation. (2004). *What is Cancer?*. Retrieved September 20th 2004 from www.us.novartisoncology.com

2. American Cancer Society. (2004). *Cancer Facts and Figures 2004*. Retrieved September 20th 2004 from http://www.cancer.org

3. Canadian Cancer Society. (2002). *Chemotherapy & You: A Guide to Self Help During Treatment.* [Brochure].

4. Bomford, C.K., Kunkler, I.H. & Sheriff, S.B. (1993). *Walter and Miller's Textbook of Radiotherapy* (5th ed.). New York, New York: Churchill Livingstone.

5. National Cancer Institute. (2004). *What is Radiation Therapy?*. Retrieved September 20th 2004 from http://www.cancer.gov

6. Perez, Carlos A., Brady, J.B. & Luther, W. (1992). *Principles and Practice of Radiation Oncology,* (2nd ed.). Philadelphia, Illinois: Lippincott.

7. Hall, Eric J. (1988). *Radiobiology for the Radiologist,* (3rd ed.). Philadelphia, Illinois: J.B. Lippincott.

8. Kriz, George S., Lampman, G.M. & Pavia, D.L. (1996). *Introduction to Spectroscopy*, (2nd ed.). Philadelphia, Illinois: Sanders College Publishing.

9. Bovey, Frank A., Mirau, P.A. & Jelinski, L. (1988). *Nuclear Magnetic Resonance Spectroscopy,* (2nd ed.). New York, New York: Academic Press.

10. Gupta, Raj K. (1987). *NMR Spectroscopy of Cells and Organisms,* (Vol. 1). Boca Raton, Florida: CRC Press.

11. Gadian, D.G. *Ann. Rev. Biophys. Bioeng.* **1983**, *12*, 69.

12. Smith, T.A.D.; Glaholm, J.; Leach, M.O.; Machin, L.; McCready, V.R. *NMR in Biomedicine* **1991,** *4*, 262.

13. Barzilai, A.; Horowitz, A.; Geier, A.; Degani, H. *Cancer* **1991,** *67*, 2919.

14. Merchant, T.E.; Meneses, P.; Gierke, L.W.; Den Otter, W.; Glonek, T. *Br. J. Cancer* **1991,** *63*, 693.

15. Merchant, T.E.; Gierke, L.W.; Meneses, P.; Glonek, T. *Cancer Research* **1988,** *48*, 5112.

Reproduced with permission of the copyright owner. Further reproduction prohibited without permission.

16. Gribbestad, I.S.; Petersen, S.B.; Fjosne, H.E.; Kvinnsland, S.; Krane, J. *NMR in Biomedicine* **1994,** *7*, 181.

17. De Graaf, Robin A. (1998). *In vivo NMR Spectroscopy*, New York, New York: John Wiley & Sons.

18. Katz-Bull, R.; Margalit, R.; Bendel, P.; Degani, H. *Magnetic Resonance Materials in Physics, Biology, and Medicine* **1998,** *6*, 44.

19. Kasimos, J.N.; Merchant, T.E.; Gierke, L.W.; Glonek, T. *Cancer Research* **1990,** *50*, 527.

20. Ruiz-Cabello, J.; Cohen, J.S. *NMR in BioMedicine* **1992**, *5*, 226.

21. Sharma, R.K.; Jain, V. *Strahlenther Onkol* **2001,** *4*, 212.

22. Voet, D.V. & Voet, J.G. (1995). *Biochemistry*, (2nd ed.). New York, New York: John Wiley & Sons.

23. Roberts, J.K.M.; Jardetzky, O. *Biochimica et Biophysica Acta* **1981**, *639*, 53.

24. Burt, C.T. (1987). *Phosphorus NMR in Biology*, Boca Raton, Florida: CRC Press.

25. Evanochko, W.T.; Ng, T.C.; Lilly, M.B.; Lawson, A.J.; Corbett, T.H.; Corbett, J.R.; Durant, J.R.; Glickson, J.D. *Proc. Natl. Acad. Sci.* **1983**, *80*, 334.

26. Furman, E.; Margalit, R.; Bendel, P.; Horowitz, A.; Degani, H. *Cancer Communications* **1991**, *3*, 287.

27. Ruiz-Cabello, J.; Berghmans, K.; Kaplan, O.; Lippman, M.E.; Clarke, R.; Cohen, J.S. *Breast Cancer Research and Treatment* **1995**, *33*, 209.

28. Sterin, M.; Cohen, J.S.; Mardor, Y.; Berman, E.; Ringel, I. *Cancer Research* **2001**, *61*, 7536.

29. Cohen, J.S.; Lyon, R.C.; Chen, C.; Faustino, P.J.; Batist, G.; Shoemaker, M.; Rubalcaba, E.; Cowen, K.H. *Cancer Research* **1986**, *46*, 4087.

30. Cohen, J.S.; Lyon, R.C. *Annals New York Acad. Of Sci.* **1987,** *508*, 216.

31. Kaplan, O.; Van Zijl, P.C.M.; Cohen, J.S. *Biochemical and Biophysical Research Communications* **1990**, *169*, 383.

32. Kaplan, O.; Kushnir, T.; Askenazy, N.; Knubovets, T.; Navon, G. *Cancer Research* **1997**, *57*, 1452.

Reproduced with permission of the copyright owner. Further reproduction prohibited without permission.

33. Sharma, R.K.; Hanssum, H.; Jain, V. *Indian Journal of Biochemistry & Biophysics* **1996,** *33*, 122.

34. Raghunand, N.; Altbach, M.I.; Van Sluis, R.; Baggett, B.; Taylor, C.W.; Bhujwalla, Z.M.; Gillies, R.J. *Biochemical Pharmacology* **1999,** *57*, 309.

35. Stubbs, M.; Bhujwalla, Z.M.; Tozer, G.M.; Rodrigues, L.M.; Maxwell, R.J.; Morgan, R.; Howe, F.A.; Griffiths, J.R. *NMR Biomed.* **1992,** *5*, 351.

36. Gillies, R.J.; Liu, Z.; Bhujwalla, Z.M. *Am. J. Physiol.* **1994,** *267*, C195.

37. Sharma, R.K.; Singh, S.; Degaonkar, M.; Raghunathan, P.; Maitra, A.; Jain, V. *Strahlenther. Onkol.* **2000,** *176*, 135.

38. Szigety, S.K.; Allen, P.S.; Huyser-Wierenga, D.; Urtasun, R.C. *Int. J. Radiation Oncology Biol. Phys.* **1993,** *25*, 695.

39. Walecki, J.; Sokol, M.; Pieniazek, P; Maeiejewski, B.; Tarnawski, R.; Krupska, T.; Wydmanski, J.; Brzezinski, J.; Grieb, P. *European Journal of Radiology* **1999,** *30*, 154.

40. Semenova, N.A.; Yushmanov, V.E.; Konradov, A.A. *NMR in Biomedicine* **1994,** *7*, 203.

41. Kallman, R.F.; Jardine, L.J.; Johnson, C.W. *J. Natl. Cancer Ins.* **1970,** *44*, 369.

42. Crau, C.; Overgaard, J. *Radiat. Res.* **1990,** *122*, 309.

43. Howes, A.E. *Br. J. Radiol.* **1969,** *42*, 441.

44. Dorie, M.J.; Kallman, R.F. *Int. J. Radiat.* **1984,** *10*, 687.

45. Dorie, M.J.; Kallman, R.F. *Int. J. Radiat. Oncol. Biol. Phys.* **1986,** *12*, 1853.

46. Gray, L.H.; Conger, A.D.; Ebert, M.; Hornsey, S.; Scott, O.C. *Br. J. Radiol.* **1953,** *26*, 638.

47. Moulder, J.E.; Rockwell, S. *Cancer Metastasis* **1987**, *5*, 313.

48. Koutcher, J.A.; Alfieri, A.A.; Barnett, D.C.; Cowburn, D.C.; Kornblith, A.B.; Kim, J.H. *Radiation Research* **1990,** *121*, 312.

49. Mahmood, U.; Alfieri, A.A.; Thaler, H.; Cowburn, D.; Koutcher, J.A. *Cancer Research* **1994,** *54*, 4885.

Reproduced with permission of the copyright owner. Further reproduction prohibited without permission.

50. Mahmood, U.; Alfieri, A.A.; Devitt, M.L.; Rhee, J.G.; Koutcher, J.A.; Kornblith, A.B.; Merchant, T.E.; Cowburn, D. *Cancer Research* **1992,** *52*, 4620.

51. Ulmer, W. *Radiobiol. Radiother.* **1990,** *31*, 313.

52. Vijayakumar, S.; Czerski, L.; Majors, A.; Valenzuela, R.; Beckett, M.; Weichselbaum, R.R.; Ng, T. *Radiobiol. Radiother.* **1992,** *52*, 5299.

53. Weichselbaum, R.R.; Beckett, M. *Int. J. Radiat. Oncol. Biol. Phys.* **1987,** *13*, 709.

54. Weichselbaum, R.R.; Dahlberg, W.; Little, J.B. *Proc. Natl. Acad. Sci. USA* **1985,** *82*, 4732.

55. Skog, S.; Tribukait, B.; Sundius, G. *Acta Radiologica Oncology* **1983,** *22*, 369.

56. Skog, S.; Tribukait, B.; Nordell, B.; Ericsson, A.; Nishida, T. *Acta Radiologica Oncology* **1986,** *25*, 63.

57. Sijens, P.E.; Wijrdemen, H.K.; Moedand, M.A. *Radiology* **1988,** *169*, 615.

58. Smith, T.A.D.; Glaholm, J.; Leach, M.O. *Br. J. Cancer* **1991,** *64*, 514.

59. Ng, T.C.; Vijayakumar, S.; Majors, A.W.; Thomas, F.J.; Meaney, T.F.; Baldwin, N.J. *Int. J. Radiation Oncology Biol. Phys.* **1987,** *13*, 1545.

60. Sijens, P.E.; Bovee, W.M.; Seijkens, D.; Los, G.; Rutgers, D.H. *Cancer Research* **1986,** *46*, 1427.

61. Merchant, T.E.; Alfieri, A.A.; Glonck, T.; Koutcher, J.A. *Radiation Research* **1995,** *142*, 29.

62. Mahmood, U.; Alfieri, A.A.; Ballon, D.; Traganos, F.; Koutcher, J.A. *Cancer Research* **1995,** *55*, 1248.

63. Cazzaniga, S.; Schold, S.C.; Sostman, H.D.; Charles, H.C. *Magnetic Resonance Imaging* **1994,** *12*, 945.

64. Aboagye, E.O.; Bhujwalla, Z.M.; He, Q.; Glickson, J.D. *Radiation Research* **1998,** *150*, 38.

65. Murata, O.; Sakural, H.; Mitsuhashi, N.; Hasegawa, M.; Yamakawa, M.; Kurosaki, H.; Hayakawa, K.; Nibe, H. *Anticancer Research* **1998,** *18*, 4297.

66. Evanochko, W.T.; Ng, T.C.; Glickson, J.D. *Magnetic Resonance in Medicine* **1984,** *1*, 508.

Reproduced with permission of the copyright owner. Further reproduction prohibited without permission.

67. Evanochko, W.T.; Sakai, T.T.; Ng, T.C.; Krishna, N.R.; Kim, H.D.; Zeidler, R.B.; Ghanta, V.K.; Brockman, R.W.; Schiffer, L.M.; Braunschweiger, P.G.; Glickson, J.D. *Biochimica et Biophysica Acta* **1984,** *805*, 104.

68. Tyagi, R.K.; Azrad, A.; Degani, H.; Salomon, Y. *Magn. Reson. Med.* **1996,** *35*, 194.

69. Folch, J.; Lees, M.; Sloan-Stanley, G.H. *Journal of Biological Chemistry* **1957,** *226*, 497.

70. Ways, P.; Hanahan, D.J. *J. Lipid Res.* **1964,** *5*, 318.

71. Glonek, T.K.; Kot, S.J.; Pettegrew, J.W.; Harrison, W.H.; Cohen, M.M. *J. Neurochem.* **1982,** *39*, 1210.

72. Barany, M. & Glonek, T. (1982). *Phosphorus-31nuclear magnetic resonance of contractile systems*, (Vol. 85). New York, New York: Academic Press.

73. Askenasy, N.; Kushnir, T.; Navon, G.; Kaplan, O. *NMR Biomed.* **1990,** *3*, 220.

74. Munch-Peterson, B.; Trysted, G.; Dupont, B. *Exp. Cell Res.* **1973,** *79*, 249.

75. Bancraft, John. D. & Stevens, A. (1996). *Theory and Practice of Histological Techniques*, (4th ed.). New York, New York: Pearson Professional.

76. Bruice, Paula Y. (1998). *Organic Chemistry*, (2nd ed.). Upper Saddle River, New Jersey: Prentice-Hall.

77. Cohn, M.; Hughes, T.R. *Journal of Biological Chemistry* **1962,** *237*, 176.

78. Meyer, E.D.; Sinclair, N.A.; Nagy, B. *Applied Microbiology* **1975,** *29*, 739.

79. Packer, E.L.; Ingraham, J.L.; Scher, S. *Journal of Bacteriology* **1965,** *89*, 718.

80. Masters, John R.W. (2000). *Animal Cell Culture*, (3rd ed.). Oxford, England: Oxford University Press.

81. Martin, Bernice M. (1994). *Tissue Culture Techniques.* Boston, Massachusetts: Braun-Brumfield Inc.

Reproduced with permission of the copyright owner. Further reproduction prohibited without permission.